AD-A280 235

WL-TR-94-1075

SENSITIVITY AND SIGNAL TO NOISE RATIO IMPROVEMENT OF A ONE MICRON LADAR SYSTEM INCOPORATING A NEODYMIUM DOPED OPTICAL FIBER PREAMPLIFIER

LASER RADAR TESTBED

Michael S. Salisbury
Electro-Optics Techniques Section
WL/AARI-2, Bldg 622
3109 P St.
Wright-Patterson AFB, OH 45433-7700

February 1994

Final Report for Period August 1991 to November 1993

DTIC
ELECTE
JUN 1 4 1994
S G D

DTIC QUALITY INSPECTED 2

Approved for public release; distribution is unlimited

AVIONICS DIRECTORATE
WRIGHT LABORATORY
AIR FORCE MATERIAL COMMAND
WRIGHT-PATTERSON AIR FORCE BASE, OH 45433-7409

94-18164

94 6 13 057

NOTICE

When Government drawings, specifications, or other data are used for any purpose other than in connection with a definitely Government-related procurement, the United States Government incurs no responsibility of any obligation whatsoever. The fact that the Government may have formulated or in any way supplied the said drawings, specifications, or other data, is not to be regarded by implication, or other wise in any manner construed, as licensing the holder, or any other person or corporation; or as conveying any right or permission to manufacture, use or sell any patented invention that may in any way be related thereto.

This report is releasable to the National Technical Information Service (NTIS). At NTIS, it will be available to the general public, including foreign nations.

This technical report has been reviewed and is approved for publication.

Michael S. Salisbury

MICHAEL S. SALISBURY, Contractor, T/SSI
Electro-Optics Techniques Group
Electro-Optics Branch

Donald L. Tomlinson

DONALD L. TOMLINSON, Chief
Electro-Optics Techniques Group
Electro-Optics Branch

Paul F. McManamon

PAUL F. McMANAMON, Acting Chief
Mission Avionics Division
Avionics Directorate

If your address has changed, if you wish to be removed from our mailing list, or if the addressee is on longer employed by your organization, please notify WL/AARI-2, Wright-Patterson AFB OH 45433-7700, to help maintain a current mailing list.

Copies of this report should not be returned unless return is required by security considerations, contractual obligations, or notice on a specific document.

REPORT DOCUMENTATION PAGE

Form Approved
OMB No. 0704-0188

Public reporting burden for this collection of information is estimated to average 1 hour per response, including the time for reviewing instructions, searching existing data sources, gathering and maintaining the data needed, and completing and reviewing the collection of information. Send comments regarding this burden estimate or any other aspect of this collection of information, including suggestions for reducing this burden, to Washington Headquarters Services, Directorate for Information Operations and Reports, 1215 Jefferson Davis Highway, Suite 1204, Arlington, VA 22202-4302, and to the Office of Management and Budget, Paperwork Reduction Project (0704-0188), Washington, DC 20503.

1. AGENCY USE ONLY *(Leave blank)*	2. REPORT DATE	3. REPORT TYPE AND DATES COVERED
	28 Feb 94	Technical Report 1 Aug 91 - 1 Nov 93

4. TITLE AND SUBTITLE Sensitivity and Signal to Noise Ratio Improvement of a One Micron Ladar System Incorporating a Neodymium Doped Optical Fiber Preamplifier. Subtitle: Final Report for In-House Laser Radar Testbed

5. FUNDING NUMBERS

PE 61101F
PR 2004
TA 08
WU 06

6. AUTHOR(S)

Michael S. Salisbury

7. PERFORMING ORGANIZATION NAME(S) AND ADDRESS(ES)

Technology/Scientific Services Inc.
P.O. Box 3065 Overlook Branch
Dayton OH 45437-3065

8. PERFORMING ORGANIZATION REPORT NUMBER

9. SPONSORING/MONITORING AGENCY NAME(S) AND ADDRESS(ES)

Avionics Directorate
Wright Laboratory
Air Force Materiel Command
Wright Patterson AFB OH 45433-7409

10. SPONSORING/MONITORING AGENCY REPORT NUMBER

WL-TR-94-1075

11. SUPPLEMENTARY NOTES

This report was prepared for WL/AARI-2 as a Masters Thesis project for the University of Dayton.

12a. DISTRIBUTION/AVAILABILITY STATEMENT

Approved for public release; distribution is unlimited.

12b. DISTRIBUTION CODE

13. ABSTRACT *(Maximum 200 words)*

In an effort to increase the signal to noise ratio of a continuous wave, one micron all solid state ladar system, a rare earth doped optical fiber amplifier has been investigated as a preamplifier for ladar return signals. This details the experimental system used and provides a theoretical analysis of the fiber amplifier's effect on heterodyne and direct detection. The SNR is plotted as a function of the return signal power, and a SNR threshold defines a minimum detectable signal power. The return signals required to attain the SNR threshold are compared for four cases: direct detection with and without the fiber amplifier, and heterodyne detection with and without the fiber amplifier. For direct detection, these results predict a sensitivity increase of 21.0 dB, yet for heterodyne detection the predicted sensitivity increase is only 4.0 dB. These SNR equations are then used to predict experimental improvements of 42.0 dB and 4.0 dB for the direct detection and heterodyne detection experiments, respectively. Experimentally measured increases in SNR are then compared to these predictions. Specifically, for direct detection a SNR increase of 36.5 dB has been measured, and for heterodyne detection the experimental work yielded an increase of 8.0 dB.

14. SUBJECT TERMS

Ladar, Lidar, Fiber Amplifier, SNR

15. NUMBER OF PAGES
73

16. PRICE CODE

17. SECURITY CLASSIFICATION OF REPORT	18. SECURITY CLASSIFICATION OF THIS PAGE	19. SECURITY CLASSIFICATION OF ABSTRACT	20. LIMITATION OF ABSTRACT
Unclassified	Unclassified	Unclassified	UL

ACKNOWLEDGMENTS

This Technical Report was prepared by the Electro-Optics Techniques Group, Electro-Optics Branch, Mission Avionics Division, Wright Laboratory, Wright-Patterson Air Force Base, Ohio.

The following personnel contributed to the formulation and review of this report:

Michael S. Salisbury, T/SSI

This Technical Report was submitted by Michael S. Salisbury in February 1994.

Accesion For	
NTIS CRA&I	☒
DTIC TAB	☐
Unannounced	☐
Justification	
By	
Distribution /	
Availability Codes	
Dist	Avail and / or Special
A-1	

PREFACE

A 1.06 micron ladar test bed has been built by the Electro-Optics Branch of the Mission Avionics Division at Wright Patterson Air Force Base. The ladar system was built with in-house research funding to evaluate experimental ladar devices as components of a ladar system. This system characterization of the devices can reveal undesirable properties of the devices early in the development phase, properties that might not be seen in a device characterization.

The Air Force Office for Scientific Research (AFOSR) funded initial work on a rare-earth doped optical fiber preamplifier by Dr. Richard Miers, Indiana University/Purdue University - Fort Wayne (IUPU-FW). The goal of the project was to investigate the effect of the fiber amplifier on ladar sensitivity by incorporating it into the one micron ladar test bed. In-house research monies at Wright Laboratory were used to provide funding for a University of Dayton graduate research assistant, who was hired through a contract with Technology/Scientific Services Incorporated (T/SSI) to develop the fiber preamplifier and incorporate it into the ladar test bed. This thesis is the result of that work effort.

TABLE OF CONTENTS

LIST OF FIGURES AND TABLES

LIST OF VARIABLES

$\hat{a}_r$	linear polarization unit vector of the return signal
$\hat{b}_{\pm f}$	random polarization unit vector of the spontaneous emission
B_e	detector electrical bandwidth
B_o	optical bandwidth of the 4 nm bandpass filter
D	heterodyne detection electronics voltage divider effect
$\vec{E}$	electric field
f	optical chopper frequency
g_a	Analog Modules electronic amplifier voltage gain
g_m	Miteq electronic amplifier voltage gain
G	fiber amplifier optical power gain
h	Planck's constant
i_r	signal current from the detector
$i_{r\text{-}se}$	return signal-spontaneous emission beat noise current
$i_{se\text{-}se}$	spontaneous emission-spontaneous emission beat noise current
i_{IF}	intermediate frequency signal current
$\langle i_n^2 \rangle$	mean squared noise current
$\langle i_d^2 \rangle$	mean squared dark current noise
$\langle i_q^2 \rangle$	mean squared shot noise current
$\langle i_t^2 \rangle$	mean squared thermal noise current
I_d	detector dark current
k	Boltzmann constant

N	number of spontaneous emission-spontaneous emission beat noise terms at 2 kHz
N_h	number of spontaneous emission-spontaneous emission beat noise terms at 200 MHz
P_r	optical return signal power incident on the detector
P_{lo}	optical local oscillator power incident on the detector
P_{se}	optical spontaneous emission power incident on the detector
$P_{se,\delta\nu}$	incremental spontaneous emission power
R_{SA}	spectrum analyzer input impedance
R_{trans}	detector package transimpedance
$\Re$	detector responsivity
$SNR_{dir,w/o}$	direct detection signal to noise ratio without the fiber amplifier
$SNR_{dir,w}$	direct detection signal to noise ratio with the fiber amplifier
$SNR_{het,w/o}$	heterodyne detection signal to noise ratio without the fiber amplifier
$SNR_{het,w}$	heterodyne detection signal to noise ratio with the fiber amplifier
t	time
T	temperature in Kelvin
V_r	signal voltage after the detector package
V_{IF}	intermediate frequency voltage
$V_{r,amp}$	signal voltage after the electronic amplifier
$V_{n,amp}$	noise voltage after the electronic amplifier
$V_{IF,amp}$	intermediate frequency voltage after the electronic amplifier
$\delta\nu$	spectrum analyzer resolution bandwidth
Δ	IF frequency
$\tilde{\Delta}_d$	predicted SNR increase for direct detection
$\tilde{\Delta}_h$	predicted SNR increase for heterodyne detection

Δ_d	experimental SNR increase for direct detection
Δ_h	experimental SNR increase for heterodyne detection
$\Phi_{\pm f}$	random phase of the spontaneous emission power
Γ_{r1}	electrical signal power for direct detection without the fiber amplifier
Γ_{r2}	electrical signal power for direct detection with the fiber amplifier
Γ_{IFa}	electrical IF power for heterodyne detection without the fiber amplifier
Γ_{IFb}	electrical IF power for heterodyne detection with the fiber amplifier
Γ_{N1}	electrical noise power for direct detection without the fiber amplifier
Γ_{N2}	electrical noise power for direct detection with the fiber amplifier
Γ_{N3}	electrical noise power for heterodyne detection without the fiber amplifier
Γ_{N4}	electrical noise power for heterodyne detection with the fiber amplifier
$\Gamma_{n,r\text{-}se}$	electrical return signal-spontaneous emission beat noise
$\Gamma_{n,lo\text{-}se}$	electrical local oscillator-spontaneous emission beat noise
$\Gamma_{n,se\text{-}se}$	electrical spontaneous emission-spontaneous emission beat noise
Γ_{ea}	electronic amplifier electrical noise power
$\eta_{opt,d}$	optical efficiency of the direct detection system between the fiber amplifier and the detector
$\eta_{opt,h}$	optical efficiency of the heterodyne detection system between the fiber amplifier and the detector
ν	bandpass filter center frequency
ω_o	angular frequency of the return signal
$\Psi_{\pm f}$	random mixing efficiency terms

CHAPTER I

INTRODUCTION

Electromagnetic waves have been used for communications since the first demonstration of radio was made by Guglielmo Marconi in 1895, shortly after Heinrich Hertz successfully generated and detected the electromagnetic waves predicted by James Clerk Maxwell. Hertz and Marconi generated the radio waves by changing the current in a wire over time, causing the wire to emit electromagnetic radiation. The wavelengths Marconi used represent the upper end of the electromagnetic spectrum, which can be divided into radio wavelengths and optical wavelengths. The radio wavelengths range from millimeters to hundreds of kilometers and are divided into microwave, short-wave radio and long-wave radio bands; the optical wavelengths range from tens of nanometers to hundreds of micrometers and are divided into ultraviolet, visible and infrared bands.[1] Radio technology pushed towards shorter wavelengths which allow larger information bandwidths, and in 1935 the German Army began to use radio for military communication systems. Shortly thereafter, radio waves were used detect and track aircraft. This technology was given the acronym of RADAR, which stands for RAdio Detection And Ranging. Radar advanced rapidly, fueled by World War I and World War II.[2]

A new method of generating electromagnetic radiation was discovered based on the quantum theory of matter. The orbital states of electrons around the nucleus of atoms give rise to radiation energy transfer as electrons shift energy levels. In 1950 MASER (Microwave Amplification by Stimulated Emission of Radiation) technology was developed, using the electron energy levels in materials such as Ruby to generate

electromagnetic waves in the microwave band.[3] Ruby was then pumped optically, which resulted in LASER (Light Amplification by Stimulated Emission of Radiation) technology. This gave coherent electromagnetic radiation at optical wavelengths with uniform wavefronts, making optical detection and ranging possible. Detection and ranging with a laser was initially designated as LIDAR (LIght Detection And Ranging), where it was understood that the source was a laser. Over time, another acronym for laser sources has become prominent, LADAR (LAser Detection And Ranging), although both acronyms are still used.[2]

Ladar and radar systems have different performance properties, and both have advantages and disadvantages in certain areas. The primary differences between the two systems are due to the nature of the emitting process and the different wavelengths. The efficiency of a ladar source is much lower than that of a radar source because of the inefficiency in obtaining ladar transmitter energy by quantum mechanical means. The wavelength dependence of ladar and radar performance results in a tradeoff between transmission and resolution properties. The long wavelengths of radar allow high transmission through the atmosphere, even when heavily cluttered with pollutants, rain, or other particles. Due to the long wavelengths, however, a radar system has very low angular resolution. On the contrary, ladar wavelengths suffer from atmospheric attenuation due to light absorption by the atmosphere and light scattering off the particles,[4] but the low wavelengths result in high angular resolution and high information bandwidths. The combination of a ladar system and a radar system can be used to obtain an optimal amount of information, but the development of ladar technology is far behind the radar technology.[5]

Ladar systems have unique applications due to some of the properties already mentioned. Remote sensing of the atmosphere is an obvious choice because of its ability to "see" particles in the atmosphere. Ladar can be used to track wind patterns such as

weather phenomena and turbulence resulting from aircraft traffic.[6,7,8,9] Pollution monitoring is another use, resulting from the optical wavelength absorption properties of particles in the air. Some pollutants will absorb certain wavelengths and reemit a spectroscopic signature, allowing contaminants to be identified and monitored remotely.[10] The angular resolution and range information capabilities of ladar lend it to a wide variety of rangefinding, tracking and targeting applications, many of which are in remote military and space based systems. [11,12,13,14] Military and space based applications create restrictions on ladar systems, particularly the laser transmitters.

Ladar technology has advanced rapidly over the years, fueled by the continual development of laser sources. The most advanced sources for ladar use gases as a lasing medium, but these sources are large and heavy, and they have a limited lifetime as the gas is slowly consumed as a result of the lasing process. Solid state lasers are more reliable, more compact and have longer lifetimes than other sources, but are less technologically developed. For the remote applications mentioned previously, these advantages are vitally important, and a large amount of research is currently underway to bring solid state lasers to the maturity level of the gas sources.[15,16,17]

Current solid state laser radar wavelengths include 1.06 μm (Nd:YAG) and recently 2.09 μm (Cr,Tm,Ho:YAG), where the parenthetical information indicates the composition of the respective laser materials.[18] These solid state systems are more efficient, have longer operating lifetimes, and are more compact and light weight than the common CO_2 ladar, which is representative of mature ladar systems with gas sources.[19]

One of the most important characteristics of any ladar system is its sensitivity. One method of increasing the sensitivity of a remote sensing device, such as a ladar system, is to optically amplify the return signal before detection. Rare earth doped optical fiber preamplifiers, highly developed by the communication industry, offer a compact and lightweight optical preamplifier for integration into a solid state ladar system. The primary

fiber amplifiers developed by the telecommunication industry are constructed using praseodymium and erbium doped fibers, for amplification at 1.3 microns and 1.55 microns respectively.[20,21] Unfortunately, these doped fibers will not amplify the return signal from a 1.064 or 2.09 micron ladar system. Neodymium doped (Nd^{3+}) optical fibers, however, have been developed for use as laser sources.[22,23] These fibers are primarily made into fiber lasers by coating or polishing the fiber ends to create a cavity. By combining the Nd^{3+} fibers used for fiber lasers and the concept of a fiber amplifier from telecommunications, an optical fiber amplifier can be developed and incorporated into a 1.064 micron ladar system, which represents mature solid state ladar technology.

When a fiber amplifier is added to a ladar receiver, the return signal is increased by a power gain factor. However, spontaneous emission from the fiber amplifier adds an optical noise to the receiver, so the benefit of the amplified return signal must be weighed against the increased noise.

Direct detection ladar systems operating at near infra-red wavelengths are limited by the noise generated by the detection electronics. In a simple, inexpensive system, these noises can be quite large. When the noise added by the fiber amplifier spontaneous emission does not have a significant impact on the overall noise of the system, a large increase in direct detection sensitivity is achieved by adding the fiber amplifier, as we will show later.

For heterodyne detection, a large local oscillator (LO) power is mixed with the return signal in order to ensure that the detection is LO shot noise limited. In this case, the spontaneous emission directly increases the shot noise. Also, the beat noise term between the spontaneous emission and the large LO has a strong impact on the noise level. Overall, the sensitivity of a heterodyne ladar system will be shown not to increase as dramatically with the addition of a fiber amplifier as the direct detection scheme.

In Chapter 2 a description of the ladar system is given, and the experimental setup used to incorporate the fiber amplifier into the system is discussed. In Chapters 3 and 4 signal to noise ratio (SNR) equations are derived for direct detection and heterodyne detection, respectively. The SNR equations for detection with and without the fiber amplifier are used in each chapter to plot SNR vs. return signal power to give a measure of the sensitivity improvement for each case. The SNR equations from Chapters 3 and 4 are also used in Chapter 5 to predict experimental SNR improvements. Experimental results are presented in Chapter 6, and Chapter 7 contains a summary and proposals for future experiments.

CHAPTER II

LADAR SYSTEM

This chapter provides an overview of the test bed ladar system, focusing on some aspects of the design that impacted the experimental work. Figures 1 and 4 show the ladar system layout for direct detection (Figure 1) and heterodyne detection (Figure 4) with the fiber amplifier inserted.

2.1 Direct Detection System

For the direct detection system, shown in Figure 1, a Nd:YAG laser, Lightwave Electronics model 120-03, provides 40 milliwatts of linearly polarized output at 1.064 microns. The laser output passes through an Electro-Optics Technology model 1845-5 Faraday optical isolator to prevent backscatter from other optical components in the system from reentering the laser head. The beam then passes through a *variable ratio attenuator* (VRA) consisting of a half wave plate in a rotatable stage and a polarizing beamsplitter cube. As will be described in detail later, this is used to reduce the transmitted optical power to levels appropriate for the targets we have used. Also note that as the photodetector we chose to use is AC coupled, the beam is modulated by a Laser Precision model CTX-534 chopper operating at 2 kHz.

After passing through the VRA, the beam passes through a *transmit/receive* (T/R) *switch*, consisting of a polarizing beamsplitter cube and an Electro-Optics Technology model 1845-5 Faraday optical rotator used to rotate the outgoing beam polarization by 45

degrees. The beam then travels to the target, after which the backscattered optical return signal received from the target is rotated an additional 45 degrees by the optical rotator. The polarization of the received signal light is thus perpendicular to the original outgoing light and is reflected by the polarizing beamsplitter cube into the return signal leg.

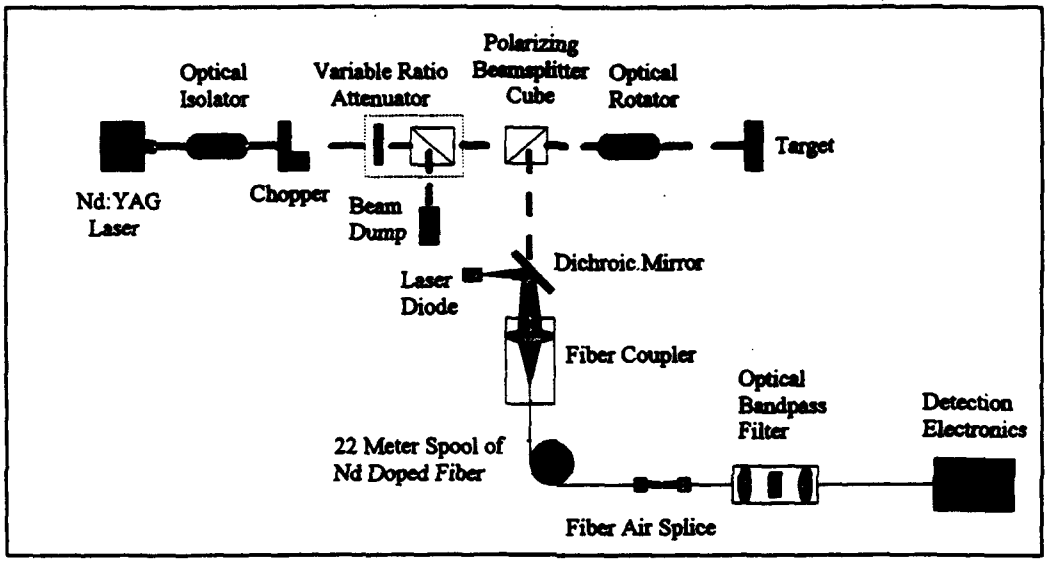

FIGURE 1: Direct Detection Ladar System. This figure shows the 1.064 micron ladar in its direct detection configuration. The variable ratio attenuator is outlined, and the fiber amplifier is shown inserted into the return signal leg.

The return signal from the target then passes through a dichroic mirror and is coupled into the core of a Rutgers University Nd^{3+} doped optical fiber, whose double cladding configuration is shown in Figure 2,[23] while pump light from a laser diode is simultaneously reflected off the dichroic mirror and coupled into the rectangular inner cladding of the doped fiber.

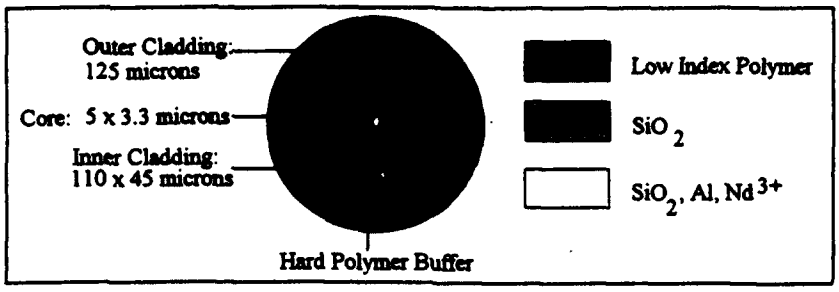

FIGURE 2: Geometry of the Rutgers Neodymium Doped Fiber. The double cladding geometry of the Rutgers fiber is shown here. The unusual rectangular inner cladding of the fiber is used to couple the pump light from a laser diode into the fiber.

Figure 3 shows in detail the setup used to couple the return signal and the pump light into the fiber amplifier.[24] The laser diode used to pump the fiber is a Laser Diode Incorporated model LDT 26010 laser diode with an 808.4 nanometer, 500 milliwatt CW output and a built in Thermo-Electric (TE) cooler. The TE cooler acts as a heat pump, which cools the laser diode emitter and decreases the output wavelength, allowing the wavelength to be tuned over a small range. The TE cooler shifts the wavelength of the laser diode to the peak absorption of the neodymium doped fiber, given to be 805 nanometers by Rutgers University. To maintain constant operating conditions, a thermistor monitors the temperature and stabilizes the output power and wavelength by using a feedback loop to vary the current to the TE cooler.

A grin rod lens from a Newport F-GRK1 graded-index rod lens kit minimizes the divergence of the output beam from the laser diode. As seen in Figure 3, the return signal and pump light are combined using a dichroic mirror, which transmits the 1.064 micron return signal and reflects the 805 nanometer pump light. The two combined beams are coupled into the fiber simultaneously using a Newport F-1015 high precision single mode fiber coupler. As the pump light travels through the fiber it passes through the core and creates a population inversion in the rare earth dopant, causing the return signal to be amplified as it passes through the core. Note that due to typically small return signals, the

fiber amplifier is operated in the small signal regime. Thus, spontaneous emission from the upper lasing level is added to the amplified return signal. We will see the effects of this spontaneous emission power later.

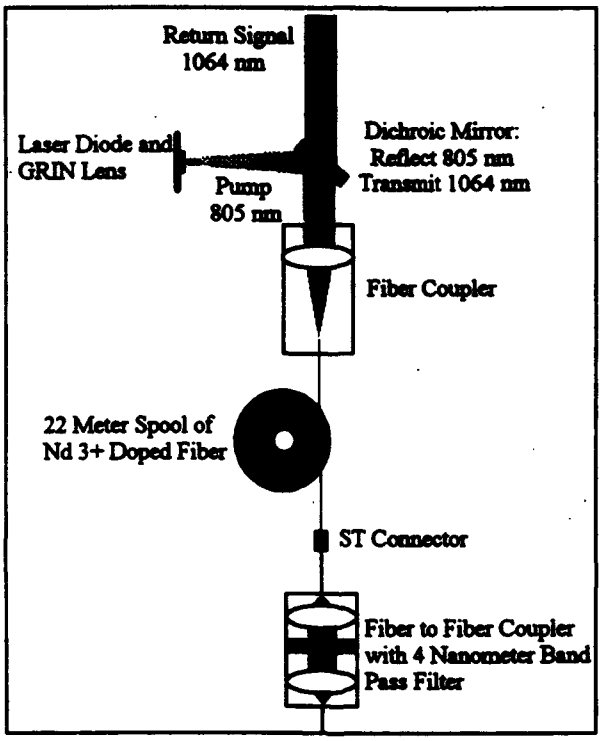

FIGURE 3: Fiber Amplifier Pump Scheme. A dichroic mirror is used to couple the pump light and the return signal light into the doped fiber. The pump is a laser diode operating at 805 nanometers, with a GRIN lens used to minimize the divergence. A four nanometer bandpass filter is inserted following the fiber amplifier to block excess pump light and to minimize the effects of spontaneous emission. The output of the bandpass filter is connected either to an evanescent wave coupler for heterodyne detection (see Figure 4) or directly to the detector for direct detection (see Figure 1).

To couple the amplified return signal out of the fiber amplifier, there is a single mode AT&T ST type connector at the end of the fiber amplifier. The double cladding geometry of the doped fiber, however, resulted in severe misalignment of the single mode

core within the ST connector which is designed for standard circular 125 micron diameter fibers. The buffer on the Rutgers fiber is made of a hard polymer, while the 125 micron outer cladding of the fiber, which would fit into the connector snugly, is made of a soft polymer. (see Figure 2) Several attempts were made to remove the buffer without stripping off the outer cladding, though all were unsuccessful. With the buffer and outer cladding removed, only the rectangular inner cladding and core are left for insertion into the connector, making it very difficult to align the core at the center of the connector. Thus, in order to couple the light out of the fiber amplifier and into another, non-doped, single mode fiber, the ST connector on the non-doped fiber was placed into a fixed mount. The connector on the end of the fiber amplifier was then fixed to a Newport three axis positioner, and index matching gel was used to provide good coupling between the fibers as the positioner was used to manually align the two cores. The resulting coupling ratios were consistently greater than 75 percent, allowing enough throughput power for experimental data to be taken.

The power coupled out of the fiber amplifier at this point includes the amplified return signal, broadband spontaneous emission power and any unabsorbed pump power. A four nanometer optical bandpass filter, centered at 1.064 microns, is used to eliminate the excess pump light (at 850 nm), as well as any spontaneous emission power outside of the $1.064 \pm .002$ micron wavelength range.

The total optical loss following the fiber amplifier for direct detection effects the amplified signal and the spontaneous emission. The two losses in the direct detection system are the air splice loss and the bandpass filter transmission loss, each contributing approximately twenty five percent. The total optical transmission of the direct detection system is thus $\eta_{opt,d} = (1-0.25)^2 = 0.56$. After the optical filter, the light is then coupled into a multimode fiber pigtailed to the InGaAs PIN detector package, from which the

output is amplified and measured with a spectrum analyzer. The amplification and detection electronics are detailed in the next chapter.

2.2 Heterodyne Detection System

For the heterodyne detection scheme shown in Figure 4, the Lightwave Electronics laser provides both the local oscillator power and the power for the transmitted signal. A half wave plate and polarizing beamsplitter cube are used as a *Variable Ratio Splitter* to vary the amount of power split into the local oscillator leg. The local oscillator is then frequency shifted 200 MHz by a model AQS-2002A1 acousto-optic modulator (AOM) from Intra-Action Corporation. The unshifted zero order beam out of the AOM is blocked with a beam dump to minimize stray reflections in the system. The frequency shifted first order is then coupled into a single mode fiber leading to an evanescent wave coupler, which couples 10 percent of the local oscillator power into the output fiber leading to the photo-detection circuitry.

Laser power not split into the local oscillator path passes through the T/R switch and is reflected off the target. The somewhat depolarized return[25] from the target passes through the T/R switch again, which directs a linearly polarized portion into the signal leg. The light reflected into the signal leg passes through a dichroic mirror and is coupled into the fiber amplifier along with the pump light from the laser diode, as discussed previously. The air splice is once again used to couple the power from the fiber amplifier into the non-doped single mode fiber leading to the free space fiber to fiber coupler, where the four nanometer band pass filter is inserted into the beam path. The optically filtered power is now coupled into the fiber leading to the evanescent wave coupler, where ninety percent is coupled into the output fiber.

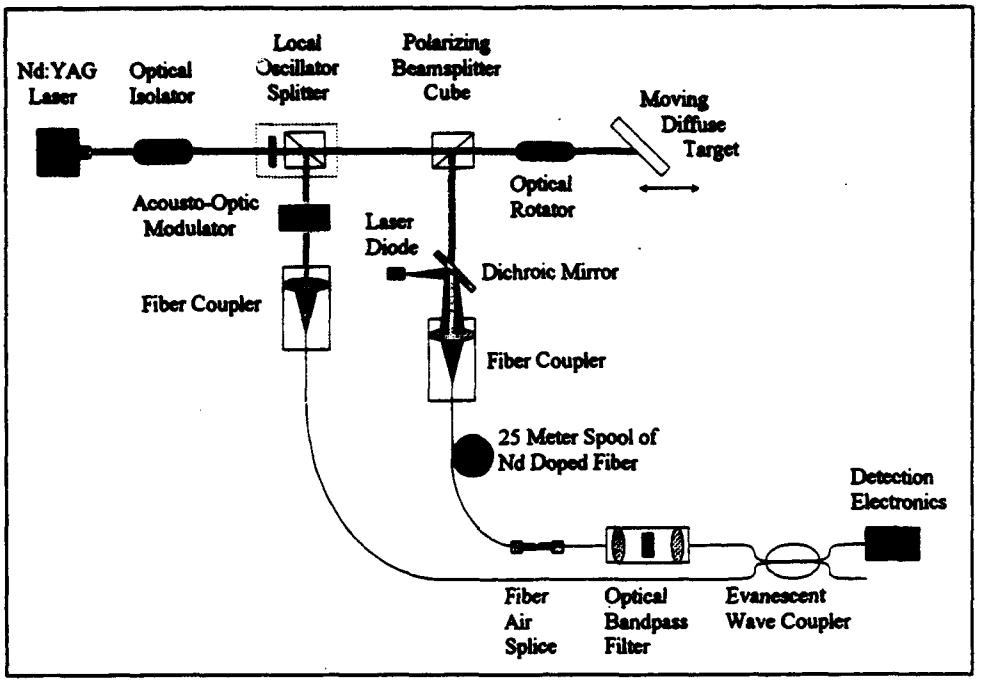

FIGURE 4: Heterodyne Detection Ladar System. This figure shows the 1.064 micron ladar in its heterodyne detection configuration. The local oscillator splitter is outlined, and the fiber amplifier is shown inserted into the return signal leg.

The total optical loss following the fiber amplifier for heterodyne detection also affects the amplified signal and the spontaneous emission. The three losses in the heterodyne detection system are the air splice loss, the bandpass filter transmission loss and the coupling loss of the evanescent wave coupler. Again, the splice and filter each contribute a loss of approximately twenty five percent, while the coupler adds a loss of ten percent to the heterodyne case. The total optical transmission of the heterodyne detection system after the fiber amplifier is thus $\eta_{opt,h} = (1\text{-}0.25)^2 \times 0.9 = 0.51$. The combined signal, local oscillator and spontaneous emission powers are then coupled into the multimode fiber pigtailed to the detection electronics, where an intermediate frequency (IF) signal at 200 MHz is generated during the photo-detection process. For heterodyne detection, the detector and electronics are detailed in Chapter 4.

2.3 Target Selection

With the system configurations thus established, the next issue became determining the targets necessary to give measurable return signals for each detection scheme. Different targets are required for the two detection schemes because of the inherent differences in the detection techniques. During direct detection the return signal is not mixed with a large local oscillator as it is in the heterodyne case. In order to generate a measurable return signal, a mirror / glint target is used as the direct detection target. The variable ratio attenuator (VRA) discussed previously (see Figure 1) is then used to vary the transmitted, and thus the received, optical power. By using the VRA in this fashion, the strength of the return signal can be adjusted until it is just visible above the noise, with the fiber amplifier not in operation. When the amplifier is turned on then, the resulting ratio of signal to noise powers yields a direct measurement of SNR improvement for the direct detection case.

For the heterodyne detection case, the large local oscillator power mixes with the return signal power to create the IF signal, thus allowing a diffuse/speckle target to be used. The driver for the acousto-optic modulator, however, radiates an electric field at the desired 200 MHz IF signal frequency. As this field tends to be picked up by the detection circuitry, resulting in a noise spike on the spectrum analyzer which drowns out the IF signal at 200 MHz, the diffuse target was mounted on a motorized linear translation stage, thus causing a small Doppler shifting of the IF signal away from the 200 MHz noise spike. More specifically, the moving diffuse target consisted of a piece of flame sprayed aluminum, tilted at 45 degrees and translated parallel to the beam path by a variable speed micrometer.

In the preliminary preparations to take measurements verifying the results of these theoretical comparisons, it is important to realize that the neodymium dopant of the fiber has a four level lasing scheme. Therefore, with the laser diode pump light blocked, the

return signal will pass through the fiber unamplified and with no loss due to signal absorption. This eliminates any need to physically remove the fiber amplifier from the system to make the signal to noise ratio comparison measurements. The signal-to-noise ratio equations in the following two chapters are developed with the goal of comparing detection sensitivity of a ladar system without and with a fiber amplifier.

CHAPTER III

SIGNAL TO NOISE RATIO THEORY FOR DIRECT DETECTION

The signal to noise ratio (SNR) is defined to be the ratio of the signal power to the noise power. This section provides a theoretical analysis of the overall post detection electronic SNR for the ladar testbed in a direct detection configuration, considering detection both with and without a fiber amplifier. The analysis begins with a discussion of the optical power incident on the detector and follows with a derivation of the signal and noise voltages after the detection electronics.

3.1 Direct Detection Without the Fiber Amplifier

For a direct detection scheme, the outgoing continuous wave laser power must be modulated so the signal current can be AC coupled into the post detection electronics. The optical chopper used to modulate the beam results in a 2 kHz square wave return signal. Figure 5 shows the electronics between the detector and the spectrum analyzer, which is used to measure the SNR. The detector is a Lasertron QDFT-250-301 pinFET detector package, with a multi-mode fiber pigtail. The photodetector is saturated at 220 microwatts of power and has a bandwidth of 250 MHz. The package includes an integrated current to voltage preamplifier with a transimpedance of 5.9 kΩ. The detector package is terminated with a 975 Ω load as a precautionary measure, as recommended by the manufacturer, and is then AC coupled to an electronic amplifier. For direct detection, the electronic amplifier is an Analog Modules 324A-3-B voltage amplifier with an input impedance of $R_{amp} = R_a = 1M\Omega$, a voltage gain $g = g_a = 1000$ and an amplification

bandwidth from 200 Hz to 35 MHz. The amplified voltage is then connected to the 50 Ohm input of a Tektronix 495P spectrum analyzer whose resolution bandwidth has been set to 10 Hz.

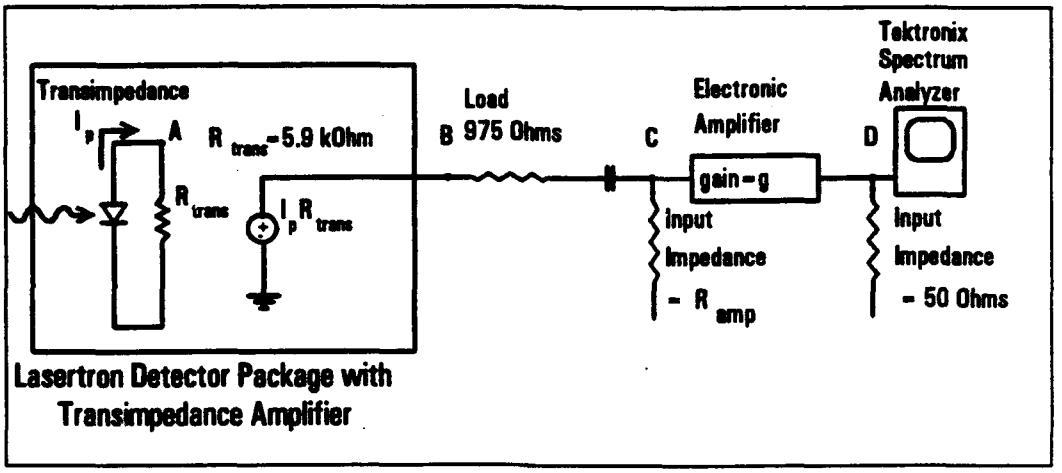

FIGURE 5: Detection Electronics. The detection electronics for the ladar system are shown here. The Lasertron detector package includes the photodetector and a current to voltage amplifier. A safety load of 975 Ohms is used to terminate the detector package. An electronic amplifier is used to boost the voltage into the spectrum analyzer used to measure the signal to noise ratio.

The signal current from the detector, i_r, at node A on Figure 5 is given by

$$i_r = \Re P_r\left[\mathrm{sqr}(2\pi f t)\right] \quad , \tag{1}$$

where $\Re$ = .704 A/W is the responsivity of the detector package, P_r is defined to be the optical return signal power *incident on the detector*, and the square wave function (sqr) in Equation 1 represents a 50% duty cycle positive square wave function (i.e. values of only zero and one). The signal voltage V_r just after the integrated preamplifier (at node B on Figure 5) is then

$$V_r = i_r R_{trans} = \Re P_r R_{trans}[\mathrm{sqr}(2\pi f t)] \quad (2)$$

where R_{trans} = 5.9 kOhm is the transimpedance of the preamplifier. The voltage is then amplified by the Analog Modules amplifier to yield a voltage at node D of

$$V_{r,amp} = g_a V_r = g_a \Re P_r R_{trans}[\mathrm{sqr}(2\pi f t)] \quad (3)$$

where due to the large input impedance of the Analog Modules amplifier, there is no appreciable voltage drop across the 975 Ohm series resistance. The signal power, Γ_{rl}, seen by the spectrum analyzer centered at 2 kHz is then

$$\Gamma_{rl} = \frac{\langle V_{r,amp}^2 \rangle}{R_{SA}} = \frac{(g_a \Re P_r R_{trans})^2 \cdot \frac{1}{2}}{R_{SA}} \quad (4)$$

where $R_{SA} = 50\Omega$ is the input impedance of the spectrum analyzer.

The total noise from the detector consists of shot noise from the optical return signal power on the detector, dark current noise and thermal noise. The well known equations for these noise components, given as mean squared noise currents, are $\langle i_q^2 \rangle = 2eB_e\langle i_r \rangle$, $\langle i_d^2 \rangle = 2eB_e I_d$, and $\langle i_t^2 \rangle = 4kB_e T/R_{trans}$, respectively, where e is the basic electronic charge, B_e is the electronic bandwidth of the detector, I_d is the detector dark current, k is the Boltzmann constant, T is the temperature in degrees Kelvin and $\langle i_r \rangle = \Re P_r/2$ is the average signal current from Equation 1.[26,27,28]

The total mean squared detector noise, $\langle i_n^2 \rangle$, is then

$$\begin{aligned}\langle i_n^2 \rangle &= \langle i_q^2 \rangle + \langle i_d^2 \rangle + \langle i_t^2 \rangle \\ &= 2eB_e\Re\left[\frac{P_r}{2}\right] + 2eB_e I_d + \frac{4kB_eT}{R_{trans}}\end{aligned} \tag{5}$$

thus yielding an average detector noise current at node A of [26]

$$\begin{aligned}\sqrt{\langle i_n^2 \rangle} &= \sqrt{\langle i_q^2 \rangle + \langle i_d^2 \rangle + \langle i_t^2 \rangle} \\ &= \sqrt{eB_e\Re P_r + 2eB_e I_d + \frac{4kB_eT}{R_{trans}}}\end{aligned} \tag{6}$$

Calculating the amplified voltage, $V_{n,amp}$, at node D yields

$$\begin{aligned}V_{n,amp} &= g_a R_{trans}\sqrt{\langle i_n^2 \rangle} \\ &= g_a R_{trans}\sqrt{eB_e\Re P_r + 2eB_e I_d + \frac{4kB_eT}{R_{trans}}}\end{aligned} \tag{7}$$

The electrical noise power seen by the spectrum analyzer is thus

$$\begin{aligned}\Gamma_n &= \frac{V_{n,amp}^{\ 2}}{R_{SA}} \\ &= \frac{\left(g_a R_{trans}\sqrt{eB_e\Re P_r + 2eB_e I_d + \frac{4kB_eT}{R_{trans}}}\right)^2}{R_{SA}}\end{aligned} \tag{8}$$

Note, though, that the noise power terms used in deriving Equation 8 are white noises in nature, so the power is equally spread across the full electrical bandwidth B_e. The spectrum analyzer noise power of Equation 8 is thus displayed as equally divided among the bandwidth intervals defined by the spectrum analyzer resolution bandwidth, $\delta\nu$ = 10

Hz. The actual noise power level displayed by the spectrum analyzer, $\Gamma_{n,\delta\nu}$, is then obtained by replacing B_e with $\delta\nu$ in Equation 8, yielding

$$\Gamma_{n,\delta\nu} = \frac{(g_e R_{trans})^2 \left(e(\delta\nu)\Re P_r + 2e(\delta\nu) I_d + \frac{4k(\delta\nu)T}{R_{trans}} \right)}{R_{SA}} \quad (9)$$

The noise power into the spectrum analyzer, however, is equal to the detector noises plus the excess noise added by the Analog Modules electronic amplifier. This noise was measured by disconnecting the detector package from the amplifier and measuring the noise level Γ_{ea} on the spectrum analyzer due to the amplifier alone. The total noise power, Γ_{N1}, is then found by adding this measured value, Γ_{ea} = -57 dBm (2 nW), to the noise in Equation 9, giving

$$\Gamma_{N1} = \Gamma_{n,\delta\nu} + \Gamma_{ea} = \frac{(g_e R_{trans})^2 \left(e(\delta\nu)\Re P_r + 2e(\delta\nu) I_d + \frac{4k(\delta\nu)T}{R_{trans}} \right)}{R_{SA}} + 2.0 \times 10^{-9} W \quad . \quad (10)$$

Using Equations 4 and 10, the direct detection SNR equation without the fiber amplifier in place is

$$SNR_{dir,w/o} = \frac{\Gamma_{r1}}{\Gamma_{N1}} = \frac{\frac{1}{2}(g_e \Re P_r R_{trans})^2}{(g_e R_{trans})^2 \left(e(\delta\nu)\Re P_r + 2e(\delta\nu) I_d + \frac{4k(\delta\nu)T}{R_{trans}} \right) + R_{SA} \cdot 2.0 \times 10^{-9} W} \quad .(11)$$

A useful measure of detection sensitivity can be obtained by plotting the SNR from Equation 11 as a function of the return signal power, P_r, as shown in Figure 6. A summary of the variables used in Equation 11 is given by Table 1.

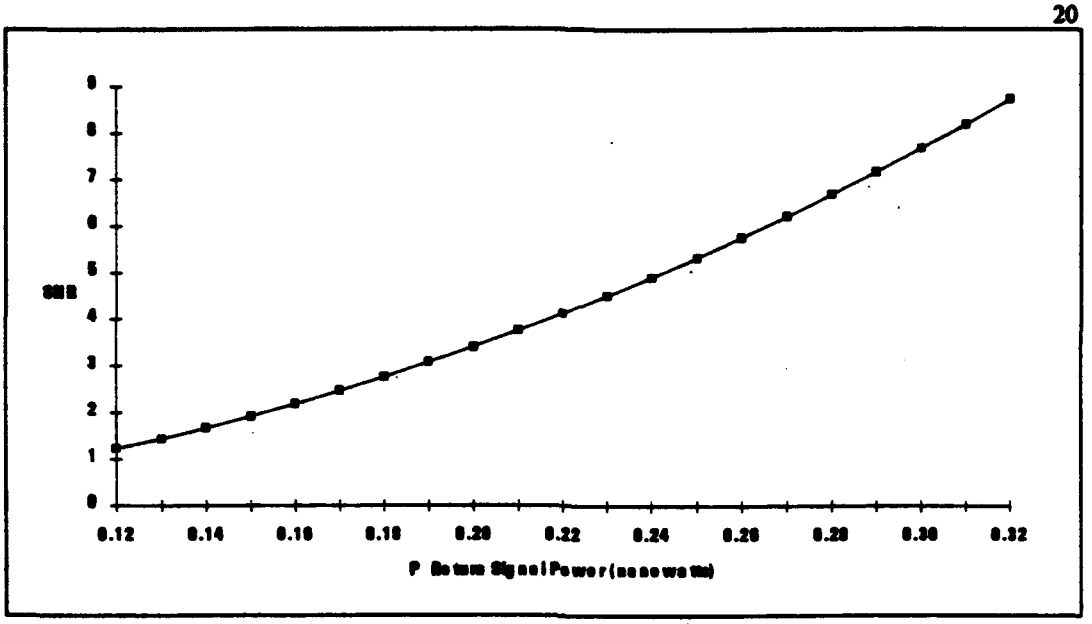

FIGURE 6: Direct Detection Signal to Noise Ratio vs. Return Signal Power for Detection Without the Fiber Preamplifier. This figure shows the signal to noise ratio as a function of return signal power for direct detection without the fiber amplifier (see Equation 11). The threshold SNR of 6 is defined to be the SNR required to discern a signal above the noise. A return signal power of 0.263 nanowatts is required to reach the threshold SNR.

This plot is used to determine the return power necessary to achieve a specified threshold SNR, defined to be the minimum SNR at which a return signal can be reliably discerned from the noise. The threshold SNR has been chosen to give a high probability of detection for normal values of the probability of false alarm.[29] From Figure 6, the minimum detectable return signal for direct detection without the fiber amplifier for the chosen threshold SNR of 6 is 0.263 nanowatts. This will be compared to the value for direct detection with the fiber amplifier, derived in the following section.

TABLE 1: List of Variable Values for use in Signal to Noise Ratio Equations. This table describes and quantifies the variables used in evaluating the signal to noise ratio equations. All variables common to both the direct and heterodyne detection equations are in the top section, while the variables distinct to either direct or heterodyne detection follow separately.

Common Variables		
ν	- Optical power center frequency (1.064 microns)	= 2.82×10^{14} Hz
$\delta\nu$	- Spectrum analyzer resolution bandwidth	= 10 Hz
B_o	- Equivalent optical passband of the 4 nm filter	= 1.07×10^{12} Hz
h	- Planck's constant	= 6.626×10^{-34} J sec
G	- Fiber amplifier power gain	= 158
R_{trans}	- Integrated amplifier transimpedance	= 5900 Ω
R_{SA}	- Spectrum analyzer input impedance	= 50 Ω
$\Re$	- Detector responsivity (Lasertron Detector)	= .704 A/Watt
e	- Basic electronic charge	= 1.6×10^{-19} C
I_d	- Detector dark current (Lasertron Detector)	= 2.9 nA
k	- Boltzmann's constant	= 1.38×10^{-23} J/K
T	- Temperature	= 298 K
Direct Detection Variables		
P_r	- Optical return signal power incident on the detector	= 0.4 nWatts
P_{se}	- Spontaneous emission power, $\eta_{opt,d}\, G\, h\, \nu\, B_o$	= 17.5 μWatts
$P_{se,\delta\nu}$	- Incremental spontaneous emission power, $\eta_{opt,d} G\, h\, \nu\, \delta\nu$	= 1.7×10^{-16} W
$\eta_{opt,d}$	- Optical efficiency between fiber amplifier and detector	= 0.56
N	- Number of se-se beat components at 2 kHz	= 1.07×10^{11}
g_a	- Analog Modules amplifier voltage gain	= 1000
R_a	- Analog Modules amplifier input impedance	= 1 MΩ
Heterodyne Detection Variables		
P_r	- Optical return signal power incident on the detector	= 8×10^{-15} Watts
P_{se}	- Spontaneous emission power, $\eta_{opt,h}\, G\, h\, \nu\, B_o$	= 15.8 μWatts
$P_{se,\delta\nu}$	- Incremental spontaneous emission power, $\eta_{opt,h} G\, h\, \nu\, \delta\nu$	= 1.5×10^{-16} W
P_{lo}	- Local oscillator power, (near detector saturation power)	= 200 μWatts
$\eta_{opt,h}$	- Optical efficiency between fiber amplifier and detector	= 0.51
g_m	- Miteq amplifier voltage gain	= 1122
D	- Voltage divider effect	= 0.048
R_m	- Miteq amplifier input impedance	= 50 Ω
N_h	- Number of se-se beat components at 200 MHz	= 1.05×10^{11}

3.2 Direct Detection With the Fiber Amplifier

For direct detection with the fiber amplifier, the return signal is increased by an optical power gain factor G. This gain factor depends on the amount of pump light absorbed and the length of the fiber. With the 500 mW laser diode pump, measured gains of 1 dB per meter have been achieved. For the 22 meter length of fiber used in the experimental work, the 22 dB gain corresponds to a power gain factor of $G = 158$. Thus the electrical signal power for direct detection with the fiber amplifier, (given by Equation 4 for direct detection without the fiber amplifier), is

$$\Gamma_{r2} = \frac{\frac{1}{2}(g_e \Re G P_r R_{trans})^2}{R_{SA}} \qquad (12)$$

The noise terms previously discussed do not change, with the exception of the shot noise term. The shot noise is larger because the signal power is now increased by a factor G and because there are also spontaneous emission photons from the fiber amplifier incident on the detector. Modifying Equation 10 accordingly, the detector noise plus electronic amplifier noise now becomes

$$\Gamma_{N2} = \frac{(g_e R_{trans})^2 \left(2e(\delta\nu)\Re\left(G\left[\frac{P_r}{2}\right] + P_{se} \right) + 2e(\delta\nu) I_d + \frac{4k(\delta\nu)T}{R_{trans}} \right)}{R_{SA}} + 2.0 \times 10^{-9}\, W \quad , (13)$$

where P_{se} is the average spontaneous emission power incident on the detector.

In general, the average spontaneous emission power is dependent on the number of contributing free space modes. For a single mode fiber amplifier, the spontaneous emission power propagating through the fiber is limited to the fraction of emitted photons coupled into the single propagating mode of the fiber. The amount of spontaneous

emission power emitted into a single mode, and thus coupled into the propagating mode, is given by [30]

$$P_{sn1} = GhvB_o \quad , \tag{14}$$

where h is Planck's constant, v is the nominal spontaneous emission frequency, and B_o is the optical bandwidth. For this case, $v = 2.82 \times 10^{14}$ is taken to be the bandpass filter center frequency, corresponding to a wavelength of 1.064 μm, and $B_O = 1.07 \times 10^{12}$ Hz is the bandwidth of the four nanometer optical bandpass filter. Note that as previously mentioned, the spontaneous emission from the fiber amplifier must pass through the connector air splice and the bandpass filter, and thus the spontaneous emission power incident on the detector is given by

$$P_{sn} = \eta_{opt,d} P_{sn1} = \eta_{opt,d} GhvB_o \quad , \tag{15}$$

where $\eta_{opt,d}$ is the fifty six percent optical efficiency of the direct detection system after the fiber amplifier.

For reasons similar to those discussed prior to Equation 9, the optical bandwidth of the spontaneous emission is broken into small frequency intervals. For convenience, the smallest measurable frequency increment is defined to be the resolution bandwidth of the spectrum analyzer. The power in a single frequency component is thus obtained by replacing B_o in Equation 15 with the spectrum analyzer resolution bandwidth δv to yield

$$P_{sn,\delta v} = \eta_{opt,d} Ghv\delta v \quad . \tag{16}$$

In addition to the increased shot noise in Equation 13, there are two additional noise terms arising as a result of spontaneous emission. The first of these terms arises due to beating between the spontaneous emission and the return signal, while the second arises due to the spontaneous emission beating with itself, both of which result from the square law detection of optical radiation.[31]

The spontaneous emission-return signal beat noise occurs when a spontaneous emission component beats with the return signal. This noise is manifest at a frequency equal to the separation between the center frequency of the return signal and the frequency of the spontaneous emission noise components. The spontaneous emission-spontaneous emission beat noise occurs between two spontaneous emission components of different frequencies. A detailed analysis of the beat noises due to spontaneous emission can be found in Appendix A of reference [31].

Only the portion of the spontaneous emission-return signal beat noise contributing to the SNR at the signal modulation frequency must be considered. This portion of the beat noise occurs when spontaneous emission components separated by +/- 2 kHz from the optical frequency of the return signal beat with the return signal. The electric field incident on the detector from the return signal and these two spontaneous emission components is [31]

$$\vec{E} = \sqrt{GP_r}\cos(\omega_o t)\hat{a}_r + \sqrt{2P_{sp,\delta\nu}}\left[\cos\left((\omega_o - 2\pi f)t + \Phi_{-f}\right)\hat{b}_{-f} + \cos\left((\omega_o + 2\pi f)t + \Phi_{+f}\right)\hat{b}_{+f}\right], \quad (17)$$

where f = 2 kHz is the signal modulation frequency, Φ_f and Φ_{-f} are the random phases for the respective spontaneous emission components, $P_{sp,\delta\nu}$ is the spontaneous emission power in one 10 Hz frequency component, $\hat{a}_r$ is the linear polarization of the return signal, $\hat{b}_{-f}$ and $\hat{b}_{+f}$ are the random polarizations of the two spontaneous emission components, and $\omega_O = 2\pi \cdot 2.82 \times 10^{14}$ is the angular frequency of the return signal. Recall now that

the detector current due to an electric field is equal to the responsivity of the detector multiplied by the squared electric field vectors such that

$$i = \Re(E)^2 \qquad (18)$$

When Equation 17 is substituted into Equation 18, two 2 kHz beat noise current terms arise from the beating between the spontaneous emission and the return signal. These terms are manipulated using trigonometric identities, resulting in the return signal-spontaneous emission beat noise current, $i_{r-sp,2kHz}$,

$$i_{r-sp,2kHz} = \Re\sqrt{2GP_r P_{sp,\delta\nu}}\left[\cos(2\pi ft + \Phi_{-f})\Psi_{-f} + \cos(-2\pi ft + \Phi_f)\Psi_f\right] \quad , (19)$$

where Ψ_{-f} and Ψ_f are random efficiency terms (i.e. $0 \le \Psi_{\pm f} \le 1$) arising due to the polarization mixing of the two fields. It is important to note that the signal bandwidth is assumed to be less than or equal to 10 Hz for this analysis. If the source has a bandwidth larger than the assumed 10 Hz, the signal power will be divided into a number of 10 Hz components. Each of these signal components will mix with spontaneous emission components, resulting in a number of beat noise terms at any frequency (i.e. 2 kHz for direct detection or 200 MHz for heterodyne detection). The total number of return signal-spontaneous emission beat noise terms at that frequency will be larger, but the magnitude of each term will be smaller. The sum of these terms results in a total beat noise term having the same magnitude as given in Equation 19, which assumed a narrowband source.

As for the spontaneous emission-spontaneous emission beat noise, the electric fields due to all spontaneous emission components must be considered, with any pair of components separated by 2 kHz contributing to the SNR noise terms at 2 kHz. The spontaneous emission electric field is represented by a summation of components,[31] each

of which is separated by the resolution bandwidth of the spectrum analyzer, $\delta\nu$ = 10 Hz, from its nearest neighboring frequency component. That is,

$$\vec{E}_{se} = \sum_{k=-M}^{M} \sqrt{2P_{se,\delta\nu}} \cos\left[(\omega_o + 2\pi k\delta\nu)t + \Phi_k\right]\hat{b}_k \quad , \qquad (20)$$

where -M and M designate spontaneous emission frequency components at the edges of the 4 nanometer ($B_o = 1.07 \times 10^{12}\,Hz$) bandpass filter. To arrive at the corresponding noise current, the squared $\vec{E}_{se}$ is multiplied by the responsivity of the detector. When the summation of Equation 20 is squared, the cross terms give rise to the spontaneous emission - spontaneous emission beat noise current, though only those beat terms affecting the SNR at 2 kHz are considered. This current is then written as a summation of those terms beating at 2 kHz, to yield

$$i_{se-se,2kHz} = \Re 2 P_{se,\delta\nu} \sum_{j=1}^{N} \left[\cos\left(2\pi f t + \Phi_j\right)\Psi_j\right] \quad , \qquad (21)$$

where Φ_j is the random phase of each beat component, Ψ_j is a term which takes into account the polarization mixing efficiency and N is the number of spontaneous emission beat terms at 2 kHz. The optical bandwidth, $B_o = 1.07 \times 10^{12}\,Hz$, contains 1.07×10^{11} of the 10 Hz frequency increments, and there are 200 frequency increments in the 2 kHz band. The total number of components separated by 2 kHz, and thus the number beating at that frequency, is obtained by $N = 1.07 \times 10^{11} - 200 \approx 1.07 \times 10^{11}$.

The beat noise currents given by Equations 19 and 21 are then analyzed through the transimpedance amplifier, the electronic amplifier and the spectrum analyzer, resulting in

$$\Gamma_{n,r-se} = \frac{\left\langle \left(g_a R_{trans} i_{r-se,2kHz} \right)^2 \right\rangle}{R_{SA}} = \frac{\left(g_a R_{trans} \Re \right)^2}{R_{SA}} G P_r P_{se,\delta\nu} \qquad (22)$$

and

$$\Gamma_{n,se-se} = \frac{\left\langle \left(g_a R_{trans} i_{se-se,2kHz} \right)^2 \right\rangle}{R_{SA}} = \frac{\left(g_a R_{trans} \Re P_{se,\delta\nu} \right)^2}{R_{SA}} N \quad , \qquad (23)$$

for the return signal-spontaneous emission and spontaneous emission-spontaneous emission beat noise power terms, respectively.

Adding the beat noise terms from Equations 22 and 23 to the detector noises from Equation 13 and including the signal power from Equation 12, the signal to noise ratio, $SNR_{dir,w}$, for direct detection with the fiber amplifier is

$$SNR_{dir,w} = \frac{\Gamma_{r2}}{\Gamma_{N2} + \Gamma_{n,r-se} + \Gamma_{n,se-se}} = \frac{\frac{1}{2}\left(g_a \Re G P_r R_{trans} \right)^2}{\left(g_a R_{trans} \right)^2 \Lambda_n + R_{SA} \cdot 2.0 \times 10^{-9} W} \quad , \qquad (24)$$

where

$$\begin{aligned} \Lambda_n &= 2e(\delta\nu)\Re\left(G\left[\frac{P_r}{2}\right] + P_{se} \right) \\ &+ 2e(\delta\nu) I_d + \frac{4k(\delta\nu)T}{R_{trans}} \\ &+ \Re^2 G P_r P_{se,\delta\nu} + \left(\Re P_{se,\delta\nu} \right)^2 N \end{aligned} \qquad (25)$$

Figure 7, a plot of SNR vs. return signal power for Equation 24, shows that the optical signal power required to reach the threshold SNR of 6 is 2.06 picowatts. (The values used in plotting Equation 23 can be found by referring to Table 1.)

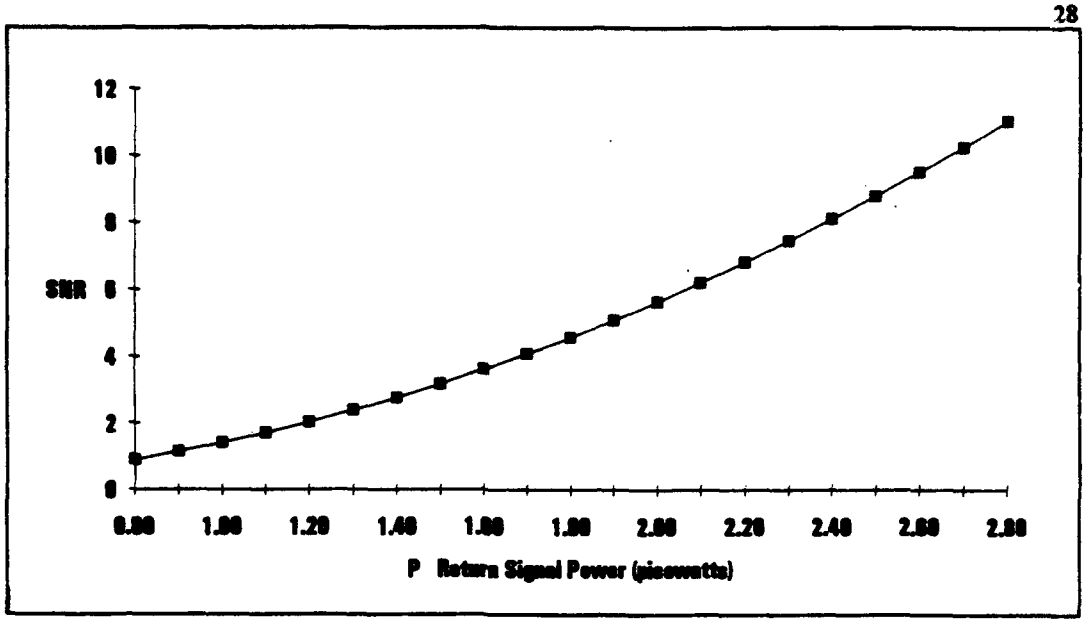

FIGURE 7: Direct Detection Signal to Noise Ratio vs. Return Signal Power for Detection With the Fiber Preamplifier. Equation 23 was used to plot the SNR as a function of return signal power for direct detection with the fiber amplifier. A return signal power of 2.06 picowatts is required to reach the threshold SNR.

The value found using Figure 7 is 21.0 dB smaller than the power required to reach the threshold for direct detection without the fiber amplifier, thus showing a significant increase in sensitivity obtained by adding the fiber amplifier to the direct detection system.[32] Next Chapter 4 compares the sensitivity of the heterodyne detection scheme with and without the fiber amplifier.

CHAPTER IV

SIGNAL TO NOISE RATIO THEORY FOR HETERODYNE DETECTION

This chapter provides a theoretical analysis of the SNR for heterodyne detection, both with and without the fiber preamplifier included. As shown, an additional noise term must be accounted for due to beating effects between the local oscillator and spontaneous emission fields. As a result of this new noise term, the sensitivity gains when using the fiber preamplifier in a heterodyne ladar system are not as dramatic as those achieved for the direct detection case.

4.1 Heterodyne Detection Without the Fiber Amplifier

The detection electronics are again given in Figure 5. The detector package is the same as used for direct detection, but a higher frequency electronic amplifier must be used to ensure amplification of the 200 MHz IF signal. The amplifier chosen is a Miteq AU-4A-0150 amplifier, with a 50 Ohm input impedance, a power gain of 61 dB and an amplification bandwidth from 1 MHz to 500 MHz.

Recall, in a heterodyne detection scheme, a local oscillator is mixed with the return signal to improve receiver sensitivity. For the test system being considered, the local oscillator is frequency shifted by an amount $\Delta = 200$ MHz. Referring back to Figure 4, the local oscillator and return signal mix at the photodetector, resulting in two DC current terms and one beat term oscillating at the 200 MHz intermediate frequency (IF). Without the fiber amplifier in place, the IF current term, i_{IF}, is written as

$$i_{IF} = \Re\left(2\sqrt{P_r P_{lo}}\cos(2\pi\Delta t)\right) \qquad (26)$$

After the integrated current to voltage preamplifier, the IF signal at node B of Figure 5 becomes

$$V_{IF} = i_{IF} R_{trans} = 2\Re R_{trans}\sqrt{P_r P_{lo}}\cos(2\pi\Delta t) \qquad (27)$$

For this detection scheme, the input impedance of the Miteq amplifier is not large enough to neglect voltage division with respect to the 975 Ω safety load resistance. The actual voltage seen by the amplifier at node C is thus reduced by a factor D, given as

$$D = \frac{50\Omega}{975\Omega + 50\Omega} = 0.048 \qquad (28)$$

The gain from the Miteq amplifier is a power gain of 61 dB, corresponding to a voltage gain of $g = g_m = 1122$. The voltage after the amplifier, $V_{IF,amp}$ at node D, is thus

$$V_{IF,amp} = g_m D V_{IF} = 2 g_m D \Re R_{trans}\sqrt{P_r P_{lo}}\cos(2\pi\Delta t) \quad , \qquad (29)$$

while the spectrum analyzer sees the following power level, Γ_{IFa}, centered at 200 MHz

$$\Gamma_{IFa} = \frac{\left\langle V_{IF,amp}{}^2 \right\rangle}{R_{SA}} = \frac{2\left(g_m D \Re R_{trans}\right)^2 P_r P_{lo}}{R_{SA}} \qquad (30)$$

The derivation of the noise power level for the heterodyne detection case without the fiber amplifier is very similar to the derivation used to obtain Equation 10. The noise power level for heterodyne detection without the amplifier, Γ_{N3}, is then

$$\Gamma_{N3} = \frac{(g_m D R_{trans})^2 \left(2e(\delta\nu)\Re(P_r + P_{lo}) + 2e(\delta\nu)I_d + \frac{4k(\delta\nu)T}{R_{trans}} \right)}{R_{SA}} + 6.3 \times 10^{-14}\, W \quad , \textbf{(31)}$$

where the electronic amplifier noise, measured for the Miteq amplifier by the same method as for the Analog Modules amplifier, was determined to be $6.3 \times 10^{-14}\, W$. *In comparison* to Equation 10, a shot noise term due to local oscillator power P_{LO} has been added, and a factor of 2 multiplying the total shot noise term has been included, as the outgoing signal is no longer chopped (see Equations 4 and 5). Also, the voltage divider effect D has been included.

For the heterodyne detection case without the fiber amplifier, it is convenient to note the limiting noises of the detection scheme. With a measured local oscillator power of 200 microwatts, the various noise terms can be evaluated to show that the local oscillator shot noise dominates the other noise factors by almost 10 dB, thus ensuring local oscillator shot noise limited detection. The noise power, under this limiting case, then becomes

$$\Gamma_{N3} = \frac{(g_m D R_{trans})^2 2e(\delta\nu)\Re P_{lo}}{R_{SA}} \qquad \textbf{(32)}$$

Taking the ratio of Equations 31 and 32 yields the signal to noise ratio, $SNR_{het.w/o}$, for heterodyne detection without the fiber amplifier, given as

$$SNR_{het,w/o} = \frac{\Gamma_{IFs}}{\Gamma_{N3}} = \frac{2(g_m D \Re R_{trans})^2 P_r P_{lo}}{(g_m D R_{trans})^2 2e(\delta\nu)\Re P_{lo}} \qquad (33)$$

Figure 8 is the plot of SNR vs. return signal power from Equation 33, again using the parameters found in Table 1. From Figure 8, 1.54×10^{-17} Watts of return signal power are required to reach the SNR threshold of 6.

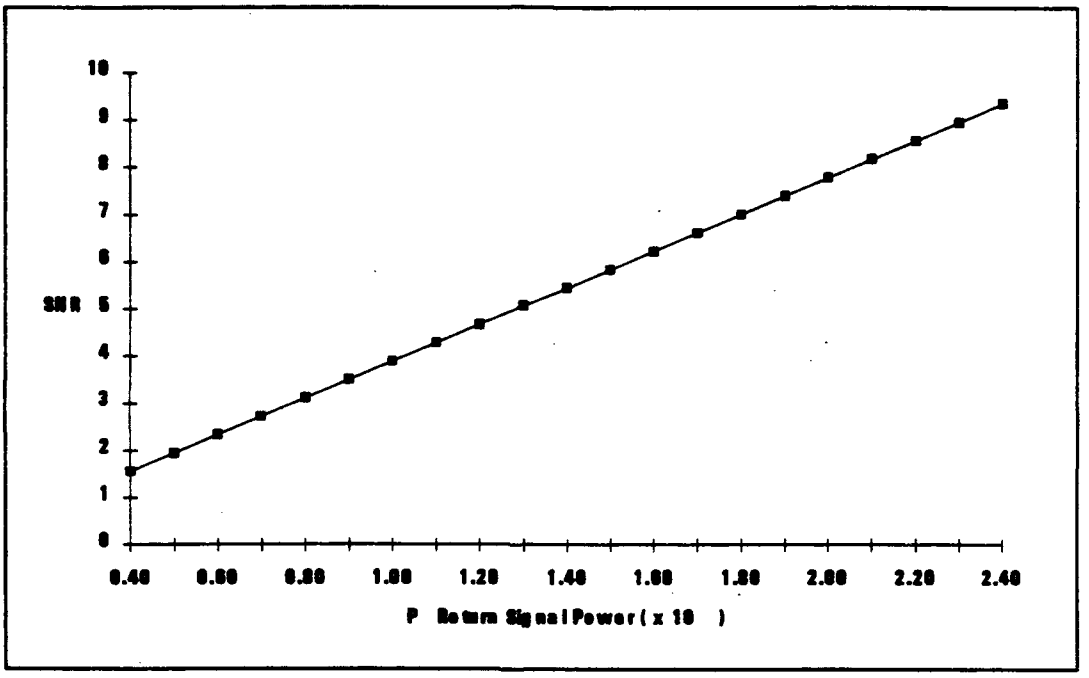

FIGURE 8: Heterodyne Detection Signal to Noise Ratio vs. Return Signal Power for Detection Without the Fiber Preamplifier. The plot shows the signal to noise ratio as a function of return signal power for heterodyne detection, without the fiber amplifier, using Equation 33. A return signal power of 1.54×10^{-17} Watts is required to reach the threshold SNR.

4.2 Heterodyne Detection With the Fiber Amplifier

For heterodyne detection with the fiber amplifier in place, the return signal is increased by the power gain factor G. The total electric field incident on the detector is composed of the amplified return signal, the local oscillator and the spontaneous emission.

The IF signal power, given by Equation 30 for heterodyne detection without the fiber amplifier, becomes

$$\Gamma_{IFb} = \frac{2(g_m D \Re R_{trans})^2 G P_r P_{lo}}{R_{SA}} \qquad (34)$$

The detector and electronic noise power level for detection with the fiber amplifier is similar to Equation 31. However, the return signal power is increased by G in the heterodyne shot noise term, and the spontaneous emission power adds another component to the shot noise term. The electronic and detector noise power level is thus

$$\Gamma_{N4} = \frac{(g_m D R_{trans})^2 \left(2e(\delta\nu)\Re(GP_r + P_{lo} + P_{se}) + 2e(\delta\nu) I_d + \frac{4k(\delta\nu)T}{R_{trans}} \right)}{R_{SA}} + 6.3 \times 10^{-14} W \quad . (35)$$

For the heterodyne case, three spontaneous emission beat noise terms must be added to Equation 35. For heterodyne detection, the spontaneous emission out of the fiber amplifier passes through the connector air splice, the bandpass filter and the evanescent wave coupler. The spontaneous emission power is therefore calculated using $\eta_{opt,h}$ and Equations 15 and 16, giving 15.8 μWatts and 1.5×10^{-16} Watts for P_{se} and $P_{se,\delta\nu}$, respectively. The first beat noise term is the return signal-spontaneous emission beat noise, given by

$$\Gamma_{n,r-se} = \frac{(\Re g_m DR_{trans})^2}{R_{SA}} 2GP_r P_{se,\delta v} \quad , \tag{36}$$

where there is a factor of two difference between this equation and the return signal-spontaneous emission beat noise of Equation 22. This factor arises because the signal power is not chopped for heterodyne detection as it is for direct detection. The second term is the local oscillator-spontaneous emission beat noise term, which has the same form as the return signal-spontaneous emission beat noise with the local oscillator power, P_{lO}, substituted for GP_r, giving

$$\Gamma_{n,lo-se} = \frac{(\Re g_m DR_{trans})^2}{R_{SA}} 2P_{lo} P_{se,\delta v} \quad . \tag{37}$$

The third term is the spontaneous emission-spontaneous emission beat noise term, given by

$$\Gamma_{n,se-se} = \frac{(\Re g_m DR_{trans})^2}{R_{SA}} P_{se,\delta v}{}^2 N_h \quad , \tag{38}$$

where N_h represents the number of beat noise terms at 200 MHz. This number is calculated similarly to the discussion proceeding Equation 21, where again there are 1.07×10^{11} incremental frequency components in B_O and 2.00×10^8 of the components in the 200 MHz band. The total number of terms beating at 200 MHz is obtained by $N = 1.07 \times 10^{11} - 2.00 \times 10^8 \approx 1.07 \times 10^{11}$. The total beat noise is thus given as [31]

$$\begin{aligned} \Gamma_{n,beat} &= \Gamma_{n,r-se} + \Gamma_{n,lo-se} + \Gamma_{n,se-se} \\ &= \frac{(\Re g_m DR_{trans})^2}{R_{SA}} \left[2GP_r P_{se,\delta v} + 2P_{lo} P_{se,\delta v} + P_{se,\delta v}{}^2 N_h \right] \end{aligned} \tag{39}$$

The SNR for heterodyne detection with the fiber amplifier is obtained from Equations 34, 35 and 39 to yield

$$SNR_{het,w} = \frac{\Gamma_{IF}}{\Gamma_{N4} + \Gamma_{n,beat}} = \frac{2(g_m D \Re R_{trans})^2 G P_r P_{lo}}{(g_m D R_{trans})^2 \Lambda_n + R_{SA} \cdot 6.3 \times 10^{-14}\, W} \quad (40)$$

where

$$\begin{aligned} \Lambda_n = {} & 2e(\delta\nu)\Re(GP_r + P_{lo} + P_{se}) \\ & + 2e(\delta\nu)I_d + \frac{4k(\delta\nu)T}{R_{trans}} \\ & + 2\Re^2 G P_r P_{se,\delta\nu} + 2\Re^2 P_{lo} P_{se,\delta\nu} \\ & + (\Re P_{se,\delta\nu})^2 N_h \end{aligned} \quad (41)$$

Figure 9 shows the SNR vs. return signal power for heterodyne detection with the fiber amplifier from Equation 40, using the values found in Table 1. The return signal power required to reach the threshold SNR is 6.0×10^{-18} Watts, giving an increase in the sensitivity of the heterodyne detection system of only 4.0 dB with the fiber amplifier added. At this point it is important to carefully examine this result, as the classical result of using optical amplification in a heterodyne detection scheme is an increase of one over the quantum efficiency of the detector.[30] This chapter's analysis appears to contradict this result, before a careful examination of the appropriate assumptions. In a heterodyne detection system, a fiber amplifier compensates for any losses after the fiber amplifier. The classical derivation assumes no losses between the optical amplifier and the detector, so the only sensitivity increase gained in adding a fiber amplifier is due to detector

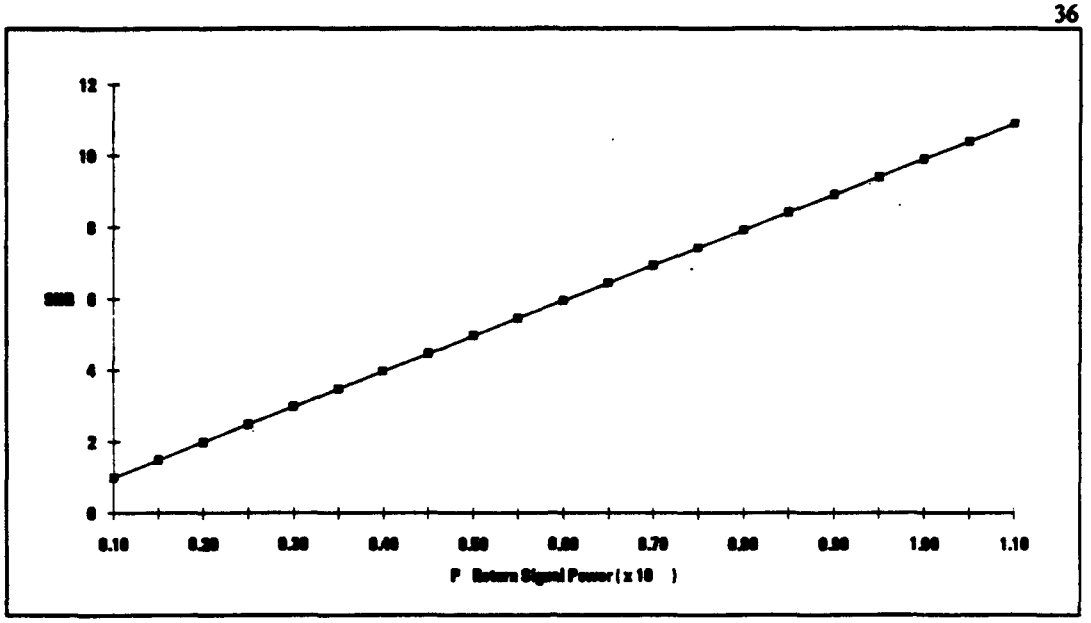

FIGURE 9: Heterodyne Detection Signal to Noise Ratio vs. Return Signal Power for Detection With the Fiber Preamplifier. Equation 40 was used to plot the SNR as a function of return signal power for direct detection with the fiber amplifier. A return signal power of 6.0×10^{-18} Watts is required to reach the threshold SNR.

inefficiency. For the ladar testbed system used, however, there is an additional optical loss after the fiber amplifier of $\eta_{opt,h}$. Including this inefficiency, the sensitivity increase is $10\log\left(1/(\eta)(\eta_{opt,h})\right) = 4.0dB$. If the optical losses are absent, the resulting increase approaches the classical result. Therefore, very little increase in sensitivity can be achieved by the addition of a fiber amplifier to an ideal heterodyne detection scheme. Chapter 5 examines the experimental measurements to be taken, and uses the equations from Chapters 3 and 4 to derive SNR improvement predictions for the experimental work.

CHAPTER V

PREDICTION OF SIGNAL TO NOISE RATIO INCREASES

The signal to noise ratio equations derived in Chapters 3 and 4 were used to determine the sensitivity increase for direct detection and heterodyne detection with the fiber amplifier. The experiments done, however, will give a measurement of the signal to noise ratio increase, not a sensitivity increase. In this chapter, the equations from the sensitivity analysis are used to predict the SNR increases for ladar detection with a fiber amplifier included. The various signal and noise terms are quantified numerically to give the predicted signal to noise ratios in dB, using the values for all parameters given previously in Table 1.

5.1 Direct Detection SNR

From Chapter 3, the signal to noise ratio for direct detection without the fiber amplifier, $SNR_{dir,w/o}$, expressed in terms of electrical power is given as

$$SNR_{dir,w/o} = \frac{\Gamma_{rl}}{\Gamma_{SN1} + \Gamma_{dark} + \Gamma_{therm} + \Gamma_{ea}} \quad , \tag{42}$$

where Γ_{rl} is the electrical signal power, Γ_{SN1} is the shot noise power, Γ_{dark} is the dark current noise power, Γ_{therm} is the thermal noise power and Γ_{ea} is the electronic amplifier noise power.

The terms in Equation 42 are related to the various system parameters given in Table 1. The electrical signal power is given by

$$\Gamma_{rl} = \frac{(1/2)(g_a \Re P_r R_{trans})^2}{R_{SA}} \quad , \tag{43}$$

where P_r is defined to be the optical return signal power incident upon the detector. This optical power is too small to be measured directly by the power meters available, so for this chapter, it is calculated by setting Equation 43 equal to the experimentally measured electrical signal power value of -45.5 dBm (see Figure 10, which we will discuss in more detail later), or 28 nW, and solving for P_r. This gives

$$P_r = \frac{(2R_{SA}\Gamma_{rl})^{1/2}}{g_a \Re R_{trans}} = 4 \times 10^{-10}\, W \quad . \tag{44}$$

Using this value for P_r the following noise terms from Equation 42 can now be evaluated:

$$\Gamma_{SN1} = \frac{(g_a R_{trans})^2 (e(\delta\nu)\Re P_r)}{R_{SA}} = 3.13 \times 10^{-16}\, W \quad , \tag{45}$$

$$\Gamma_{dark} = \frac{(g_a R_{trans})^2 (2e(\delta\nu) I_d)}{R_{SA}} = 4.45 \times 10^{-15}\, W \quad , \tag{46}$$

$$\Gamma_{therm} = \frac{(g_a R_{trans})^2 (4k(\delta\nu)T/R_{trans})}{R_{SA}} = 1.9 \times 10^{-11}\, W \quad . \tag{47}$$

where e is the basic electron charge, $\delta\nu$ is the resolution bandwidth of the spectrum analyzer, I_d is the detector dark current, k is the Boltzmann constant and T is the

temperature in Kelvin. Note that the electronic amplifier noise power of Equation 42 is a measured value. To perform this measurement, the electronic amplifier input was disconnected from the detector package, and the output was measured on the spectrum analyzer, resulting in a measured amplifier noise value of

$$\Gamma_{ea} = 2.0 \times 10^{-9} W \tag{48}$$

As seen then from Equations 45 - 48, the measured electronic amplifier noise level of $2 \times 10^{-9} W$ or -57 dBm, is much larger than the other noise terms, thus allowing Equation 42 to be evaluated as follows

$$SNR_{dir,wo} = \frac{2.8 \times 10^{-8} W}{2 \times 10^{-9} W} = 14.0 \ (11.5 \text{ dB}) \tag{49}$$

Similar to Equation 42, the signal to noise ratio for direct detection with the fiber amplifier, $SNR_{dir,w}$, is

$$SNR_{dir,w} = \frac{\Gamma_{r2}}{\Gamma_{SN2} + \Gamma_{n,r-se} + \Gamma_{n,se-se} + \Gamma_{ea}} \tag{50}$$

where Γ_{r2} is the signal power, Γ_{SN2} is the shot noise power, $\Gamma_{n,r\text{-}se}$ is the return signal-spontaneous emission beat noise power, $\Gamma_{n,se\text{-}se}$ is the spontaneous emission-spontaneous emission beat noise power and Γ_{ea} is the electronic amplifier noise power. Specifically, these terms are

$$\Gamma_{r2} = \frac{(1/2)(g_a \Re G P_r R_{trans})^2}{R_{SA}} \tag{51}$$

$$\Gamma_{SN2} = \frac{(g_e R_{trans})^2 \left(2e(\delta\nu)\Re\left(G \cdot \frac{P_r}{2} + P_{se} \right) \right)}{R_{SA}} \quad (52)$$

$$\Gamma_{n,r-se} = \frac{(g_e R_{trans})^2 (\Re^2 G P_r P_{se,\delta\nu})}{R_{SA}} \quad (53)$$

$$\Gamma_{n,se-se} = \frac{(g_e R_{trans})^2 (\Re P_{se,\delta\nu})^2}{R_{SA}} N \quad (54)$$

$$\Gamma_{as} = 2.0 \times 10^{-9} W \quad , \quad (55)$$

where the new terms in these equations are the fiber amplifier gain, G, the total spontaneous emission power, P_{se}, the incremental spontaneous emission power, $P_{se,\delta\nu}$, and N, the number of spontaneous emission terms beating at the 2 kHz chopper frequency within the equivalent bandwidth of the 4 nm optical band pass filter.

Using the previously determined 1 dB/m small signal gain of the Rutgers fiber, the 22 m length of fiber used in the experiment gives approximately 22 dB of gain, or G = 158. With this length of fiber and this gain, the spontaneous emission power incident on the detector after the air splice and optical bandpass filter (from Equation 15) is

$$P_{se} = \eta_{opt,d} G h\nu B_o = 17.5 \mu W \quad . \quad (56)$$

Using the optical signal power, the spontaneous emission power and the fiber amplifier gain, the shot noise power Γ_{SN2} is then calculated from Equation 52 to be

$$\Gamma_{SN2} = 2.78 \times 10^{-11} W \qquad (57)$$

The incremental spontaneous emission power, from Equation 16, is calculated to be

$$P_{se,\delta\nu} = \eta_{opt,d} G h \nu \delta\nu = 1.7 \times 10^{-16} \qquad (58)$$

$\Gamma_{n,r\text{-}se}$ is then determined to be

$$\Gamma_{n,r-se} = 3.61 \times 10^{-12} W \quad , \qquad (59)$$

while the spontaneous emission-spontaneous emission beat noise term, $\Gamma_{n,se\text{-}se}$, is found to be

$$\Gamma_{n,se-se} = 1.05 \times 10^{-9} W \quad , \qquad (60)$$

thus giving a total noise level Γ_N for direct detection with the fiber amplifier of

$$\Gamma_N = \Gamma_{SN2} + \Gamma_{n,r-se} + \Gamma_{n,se-se} + \Gamma_{ss} = 3.1 \times 10^{-9} W \qquad (61)$$

This corresponds to a noise level of -55.1 dBm.

The predicted SNR for direct detection with the fiber amplifier is then found by substituting Equations 11 and 21 into Equation 10, giving

$$SNR_{dir,w} = \frac{\Gamma_{r2}}{\Gamma_N} = \frac{6.9 \times 10^{-4}}{3.1 \times 10^{-9}} = 222581 \quad , \qquad (62)$$

which corresponds to a SNR of 53.5 dB. The predicted direct detection increase in signal to noise ratio, $\tilde{\Delta}_d$, can then be obtained by subtracting (in dB) the SNR without the fiber amplifier from the predicted increase with the fiber amplifier, giving

$$\begin{aligned}\tilde{\Delta}_d &= 53.5dB - 11.5dB \\ &= 42.0dB\end{aligned} \tag{63}$$

5.2 Heterodyne detection SNR

For heterodyne detection without the fiber amplifier, the SNR equation, $SNR_{het,w/o}$, is given by

$$SNR_{het,w/o} = \frac{\Gamma_{IFa}}{\Gamma_{SN3}} \quad , \tag{64}$$

where Γ_{IFa} is the intermediate frequency (IF) electrical signal power and Γ_{SN3} is the local oscillator shot noise power, where we assume that the local oscillator power has been increased until the LO shot noise term dominates all other noises. From Chapter 4, these terms are given by

$$\Gamma_{IFa} = \frac{2(g_m D \Re R_{trans})^2}{R_{SA}} P_r P_{lo} \tag{65}$$

and

$$\Gamma_{SN3} = \frac{(g_m D R_{trans})^2}{R_{SA}} 2e(\delta\nu)\Re P_{lo} \tag{66}$$

The IF electrical signal power for heterodyne detection without the fiber amplifier was measured (see Figure 12) to be -55 dBm, or 3.2 x 10^{-9} W. This allows the received optical power for heterodyne detection, P_r, to be calculated from Equation 65, yielding

$$P_r = \frac{R_{SA}\Gamma_{IFo}}{2P_{lo}\left(g_m D R_{trans}\Re\right)^2} = 8.0\times10^{-15}\,W \quad . \tag{67}$$

This value for P_r is used to predict the signal to noise ratio for heterodyne detection with the fiber amplifier.

Continuing our analysis for heterodyne detection without the fiber amplifier, however, the local oscillator shot noise power, Γ_{SN3}, was calculated from Equation 66 to be

$$\Gamma_{SN3} = 9.15\times10^{-13}\,W \quad , \tag{68}$$

corresponding to a noise level of -90.1 dBm. This value is approximately 10 dB larger than the electronic noise from the Miteq amplifier, which was measured to be 6.4×10^{-14} W, or -101.9 dBm, thus verifying that our heterodyne detection system was indeed local oscillator shot noise limited. The predicted SNR for heterodyne detection without the fiber amplifier is therefore

$$SNR_{het,w/o} = \frac{\Gamma_{IFo}}{\Gamma_{SN3}} = \frac{3.2\times10^{-9}\,W}{9.9\times10^{-13}\,W} = 3238.8\ (35.0\text{dB}) \quad . \tag{69}$$

We now consider the case of heterodyne detection with the fiber amplifier, where the signal to noise ratio equation, $SNR_{het,w}$, is given by

$$SNR_{het,w} = \frac{\Gamma_{IFb}}{\Gamma_{SN4} + \Gamma_{n,r-se} + \Gamma_{n,lo-se} + \Gamma_{n,se-se}} \quad , \qquad (70)$$

where Γ_{IFb} is the amplified IF signal power, Γ_{SN4} is the shot noise term when the fiber amplifier is included, $\Gamma_{n,r\text{-}se}$ is the return signal-spontaneous emission beat noise power, $\Gamma_{n,lo\text{-}se}$ is the local oscillator-spontaneous emission beat noise power, and $\Gamma_{n,se\text{-}se}$ is the spontaneous emission-spontaneous emission beat noise power. From Chapter 4, these terms are as follows:

$$\Gamma_{IFb} = \frac{2(g_m D \Re R_{trans})^2}{R_{SA}} G P_r P_{lo} \qquad (71)$$

$$\Gamma_{SN4} = \frac{(g_m D R_{trans})^2}{R_{SA}} 2e(\delta\nu)\Re(P_{lo} + P_{se}) \qquad (72)$$

$$\Gamma_{n,r-se} = \frac{(g_m D R_{trans})^2}{R_{SA}} 2\Re^2 G P_r P_{se,\delta\nu} \qquad (73)$$

$$\Gamma_{n,lo-se} = \frac{(g_m D R_{trans})^2}{R_{SA}} 2\Re^2 P_{lo} P_{se,\delta\nu} \qquad (74)$$

$$\Gamma_{n,se-se} = \frac{(g_m D R_{trans})^2}{R_{SA}} (\Re P_{se,\delta\nu})^2 N_h \quad , \qquad (75)$$

where N_h is the number of spontaneous emission components beating together at the heterodyne frequency. (See Table 1)

Using Equation 73, the return signal-spontaneous emission noise is calculated to be

$$\Gamma_{n,r-se} = 7.66 \times 10^{-19} W \quad . \tag{76}$$

Similarly, using Equation 74, the local oscillator-spontaneous emission beat noise is found to be

$$\Gamma_{n,lo-se} = 6.06 \times 10^{-11} W \quad , \tag{77}$$

while the spontaneous emission-spontaneous emission beat noise from Equation 75 is found to be

$$\Gamma_{n,se-se} = 2.44 \times 10^{-12} W \quad , \tag{78}$$

thus giving a total noise level, Γ_N, of

$$\Gamma_N = \Gamma_{SN4} + \Gamma_{n,r-se} + \Gamma_{n,lo-se} + \Gamma_{n,se-se} = 6.4 \times 10^{-11} W(-71.9 dBm) \quad . \tag{79}$$

The predicted signal to noise ratio for heterodyne detection with the fiber amplifier is then found by substituting Equations 71 and 79 into Equation 70, giving

$$SNR_{het,w} = \frac{\Gamma_{IFb}}{\Gamma_{SN4} + \Gamma_{n,r-se} + \Gamma_{n,lo-se} + \Gamma_{n,se-se}} = \frac{5.06 \times 10^{-7}}{6.4 \times 10^{-11}} = 7906(39.0 dB) \quad . \tag{80}$$

The predicted SNR increase for heterodyne detection with the fiber amplifier, $\tilde{\Delta}_h$, is then obtained by subtracting (in dB) the SNR for heterodyne detection without the fiber amplifier from the SNR for heterodyne detection with the fiber amplifier, giving

$$\begin{aligned} \tilde{\Delta}_h &= 39.0dB - 35.0dB \\ &= 4.0dB \end{aligned} \tag{81}$$

In Chapter 6, the experimental data is given and compared to the results of this analysis.

CHAPTER VI

EXPERIMENTAL DATA

In this section we present the SNR data we have taken and make comparisons between our measurements and the predicted values found in the previous sections. The first data taken was for direct detection without the fiber amplifier. Figure 10 shows the spectrum analyzer display for this case, where we note that the average noise level is -57 dBm, which is equal to the measured value for the electronic amplifier (Analog Modules amplifier) noise discussed in Chapter 3.

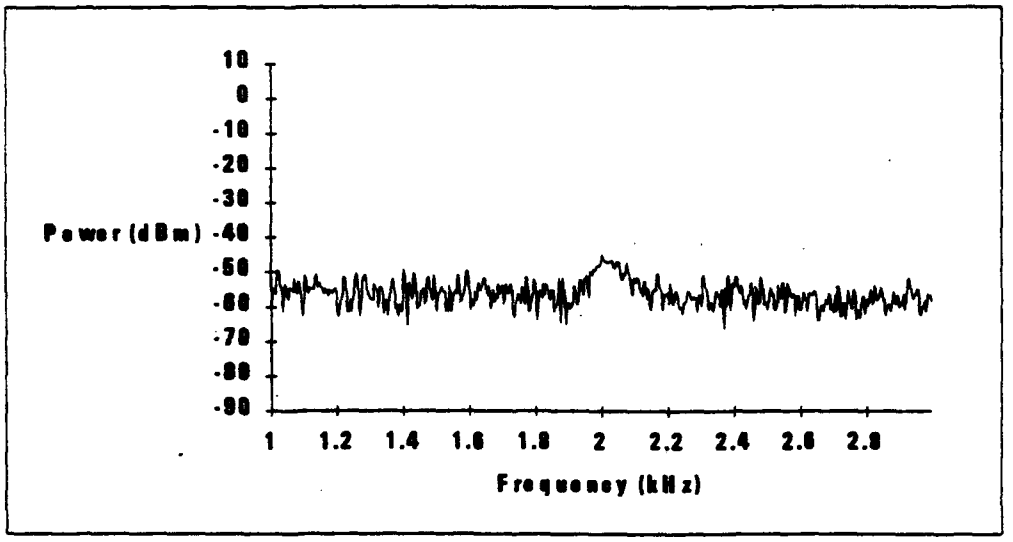

Figure 10 Experimental Signal to Noise Ratio Data : Direct Detection Without the Fiber Preamplifier. This figure shows data taken from the spectrum analyzer for direct detection without the fiber amplifier turned on. The direct detection signal is located at 2 kHz. The noise level is -57.0 dBm and the signal level is -45.5 dBm, giving a SNR of 11.5 dB.

This verifies our limiting noise assumption for direct detection without the fiber amplifier. Also, the signal level in Figure 10 is seen to be -45.5 dBm, which is the value used in Equation 44 to calculate the optical return signal power. The measured SNR is thus 11.5 dB.

Figure 11 is a plot of the signal and noise for direct detection with the fiber amplifier turned on. The electrical signal power level is seen to be -1.1 dBm, while the noise level is -49.1 dBm, giving an experimental SNR of 48.0 dB.

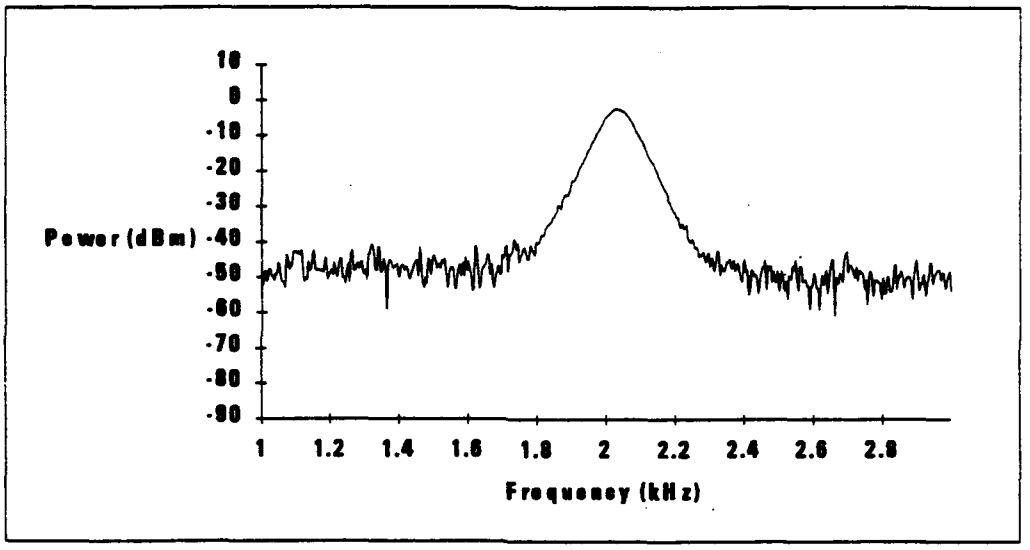

Figure 11 Experimental Signal to Noise Ratio Data : Direct Detection With the Fiber Preamplifier. This figure shows data taken from the spectrum analyzer for direct detection with the fiber amplifier. The direct detection signal is located at 2 kHz. The noise level is -48.6 dBm and the signal level is -2.2 dBm, giving a SNR of 46.4 dB.

The experimental increase in SNR for direct detection with the fiber amplifier, Δ_d, is then obtained by subtracting (in dB) the SNR without the fiber amplifier from the SNR with the fiber amplifier

$$\Delta_d = 48.0dB - 11.5dB = 36.5dB \quad (82)$$

This measured SNR increase is 5.5 dB smaller than the increase of 42.0 predicted in Section 5.1. In examining the error, it is seen that there are several errors inherent in the spectrum analyzer used. From the specifications given in the operators manual, errors in the Display Dynamic Range Accuracy, RF Attenuator Range Accuracy and IF Gain Range Accuracy are ± 2 dB, ±1 dB and ± 2 dB, respectively, giving a possible cumulative error of ± 5 dB. These errors, combined with small, unavoidable experimental uncertainties, can account for the 5.5 dB difference in the predicted SNR and experimental SNR.

Next, Figure 12 shows the Doppler shifted IF signal, located at 199.9982 MHz, for heterodyne detection without the fiber amplifier.

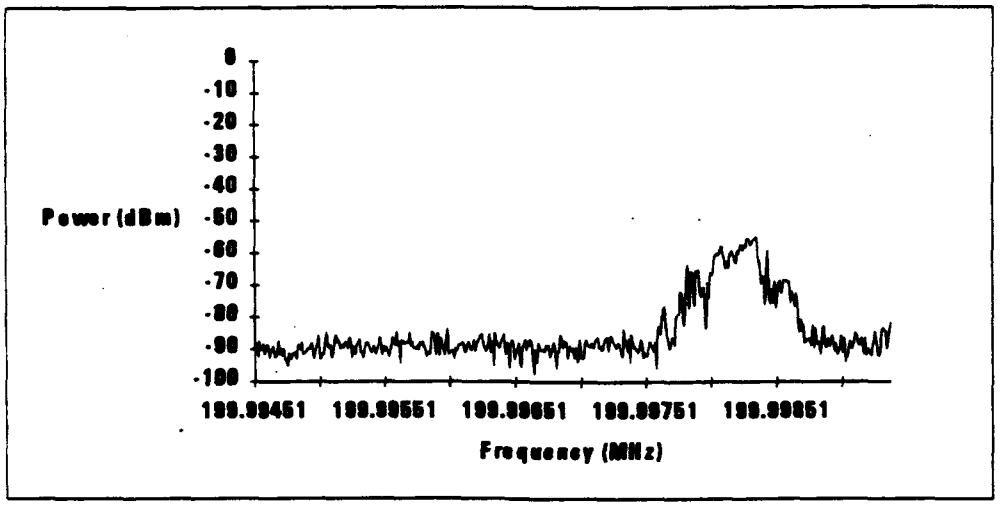

Figure 12 Experimental Signal to Noise Ratio Data : Heterodyne Detection Without the Fiber Preamplifier. This figure shows data taken from the spectrum analyzer for heterodyne detection without the fiber amplifier. The heterodyne detection signal is located at 199.9982 MHz. The noise level is -90.4 dBm and the signal level is -55.0 dBm, giving a SNR of 36 dB.

The electrical signal power is seen to be -55 dBm, as was used to calculate the optical return signal in Equation 67. The noise level is also seen to be -91 dBm, which is approximately the calculated local oscillator shot noise power described in Section 3.2. These values give a SNR of 36 dB for heterodyne detection without the fiber amplifier.

Figure 13 is a plot of the signal and noise for heterodyne detection with the fiber amplifier turned on. The electrical signal power level is -33 dBm, while the noise level is -77 dBm, giving an experimental SNR of 44 dB.

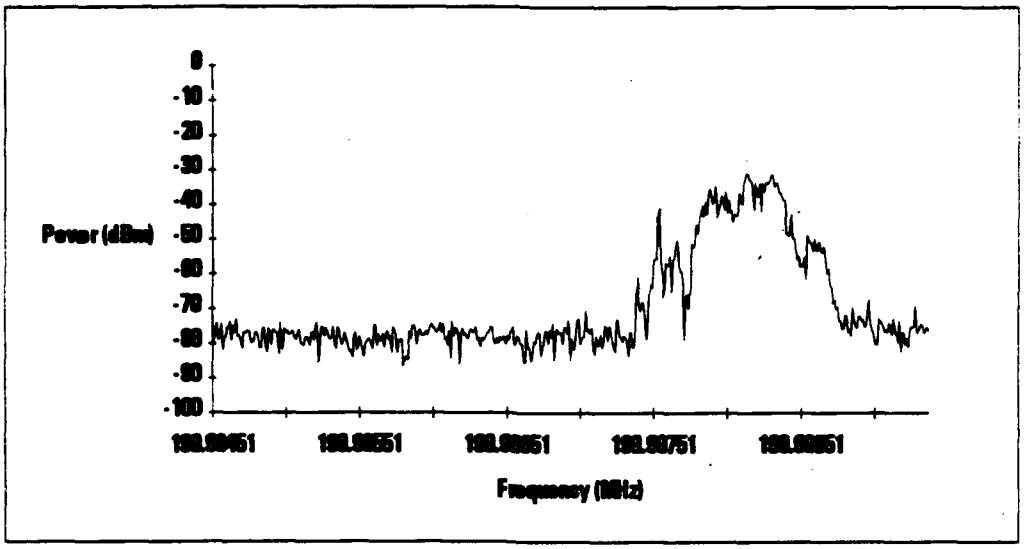

Figure 13 Experimental Signal to Noise Ratio Data : Heterodyne Detection With the Fiber Preamplifier. This figure shows data taken from the spectrum analyzer for heterodyne detection with the fiber amplifier. The heterodyne detection signal is located at 199.9982 MHz. The noise level is at -77.0 dBm and the signal level is -33.0 dBm, giving a SNR of 44 dB.

The experimental increase in SNR for heterodyne detection with the fiber amplifier, Δ_A, is obtained by subtracting (in dB) the SNR without the fiber amplifier from the SNR with the fiber amplifier to yield

$$\Delta_h = 44dB - 36dB = 8dB \tag{83}$$

The measured increase in SNR is 4.0 dB larger than the predicted increase of 4.0 dB. The ± 5 dB uncertainty in the display accuracy of the spectrum analyzer is again sufficient to account for the difference between the predicted and experimental SNR increases.

In comparing the direct and heterodyne detection results, it is somewhat disconcerting to see experimental results smaller than predicted for one case and larger than predicted in the other. This result is caused by the different power levels used by the two detection schemes. Specifically, the noise and amplified signal levels for the direct detection case are very near the maximum range of the spectrum analyzer, while the heterodyne detection noise floors are near the minimum sensitivity level of the spectrum analyzer. These two extremes represent the difference between ± 5 dB in the accuracy, and it is reasonable to expect the experimental differences of the two cases to have opposite signs.

CHAPTER VII

CONCLUSIONS AND RECOMMENDATIONS

A neodymium doped optical fiber amplifier has been incorporated into a solid state ladar test bed to determine its effect on the sensitivity and signal to noise ratio of the system. The design incorporating the fiber amplifier into the test bed was described in detail, and some of the difficulties in implementing this were noted. A theoretical model of the electrical signal and noise powers were developed for direct detection and heterodyne detection. These equations were then used to predict the sensitivity increases achieved by adding a fiber amplifier to each detection scheme. These same equations were used to predict the signal to noise ratio increases that would be seen experimentally by adding the fiber amplifier to the system. Measurements were then taken with the ladar system to verify the validity of the theoretical model.

For the direct detection case, the measured SNR increase for detection with the fiber amplifier was 36.5 dB, which is 5.5 dB less than the predicted increase of 42.0 dB. For heterodyne detection, the measured SNR increase is 8.0 dB, which is 4.0 dB larger than the predicted increase of 4.0 dB.

Further work in this area is recommended to examine fiber amplifier performance in true ladar functions such as ranging and target detection. This includes examining the effect of the fiber amplifier on return signals resulting from a pulsed or chirped output. The research should also expand into eyesafe wavelengths, such as erbium doped fibers at 1.54 microns, which will take advantage of the advanced technology driven by the communication industry.

APPENDIX A

THE DESCRIPTION OF PHOTON NOISE THROUGH POISSON STATISTICS

This appendix discusses how Poisson statistics may be used to describe shot noise in the photon detection process.

In describing the photon detection process, the detector is assumed to be an ideal photon detector. This assumes there is no current from the detector in the absence of incident light and there is no noise from detector imperfections or the detector electronics. The light incident on the detector is laser light, which has constant power and nearly monochromatic light of frequency ν, adding no noise to the detection process. The noise from the detection process is considered to arise from a randomness in the emission times of photoelectrons from the detector.

Since photon detection is a discrete physical process, it can be described by Poisson statistics. For Poisson statistics the probability distribution function $P_T(n)$ is defined to be the probability n photons will be detected in a sample time interval of T. An important quantity in the Poisson probability distribution function is $\langle n \rangle$, the average number of photon events in T. This quantity is arrived at by taking a large number of time samples and finding the average n. The Poisson probability distribution function is given in terms of n and $\langle n \rangle$ by Equation A.1 [1]

$$P_T(n) = \frac{\langle n \rangle^n}{n! e^{\langle n \rangle}}. \qquad \text{A.1}$$

Figure A.1 is a plot of n versus $P_T(n)$ for an $\langle n \rangle$ given to be 10. It is used to determine the probability n photons will be detected in any interval T.

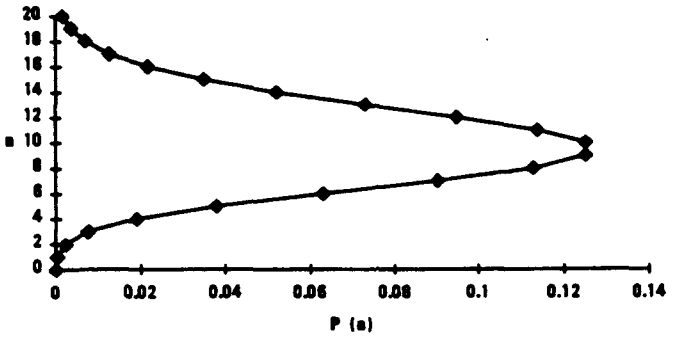

Figure A.1 A plot of the number of photons versus probability of that number of photons being detected in a time interval T. The plot is made using Equation A.1 with an <n> of 10.

Now that the statistics of the detection process have been expressed, it is necessary to give the definition of noise. The quantity of interest is the variance, σ^2, defined to be the mean square noise level. The variance of any process can be calculated from Equation A.2 [2]

$$\sigma^2 = \left\langle (n - \langle n \rangle)^2 \right\rangle. \qquad \text{A.2}$$

Equation A.2 can be simplified to

$$\begin{aligned} \sigma^2 &= \left\langle (n - \langle n \rangle)^2 \right\rangle = \left\langle n^2 - 2n\langle n \rangle + \langle n \rangle^2 \right\rangle \\ &= \left\langle n^2 \right\rangle - \left\langle 2n\langle n \rangle \right\rangle + \left\langle \langle n \rangle^2 \right\rangle \\ &= \left\langle n^2 \right\rangle - \langle n \rangle^2 \end{aligned} \qquad \text{A.3}$$

For a Poisson process, Equation A.3 can be used to show the variance is equal to the mean. This derivation, from Boyd, starts with the algebraic identity

$$n^2 = n + n(n-1). \qquad \text{A.4}$$

Then

$$\begin{aligned} \langle n^2 \rangle &= \langle n + n(n-1) \rangle \\ &= \langle n \rangle + \langle n(n-1) \rangle \end{aligned} \qquad \text{A.5}$$

Using the statistical definition of $\langle n(n-1) \rangle$,

$$\langle n(n-1) \rangle = \sum_{n=0}^{\infty} n(n-1) P_T(n) \qquad \text{A.6}$$

Equation A.5 becomes

$$\begin{aligned} \langle n^2 \rangle &= \langle n \rangle + \sum_{n=0}^{\infty} n(n-1) P_T(n) \\ &= \langle n \rangle + \sum_{n=0}^{\infty} n(n-1) \frac{\langle n \rangle^n e^{-\langle n \rangle}}{n!} \end{aligned} \qquad \text{A.7}$$

The n=0 and n=1 terms of the summation in Equation A.7 are equal to zero

$$\langle n^2 \rangle = \langle n \rangle + \sum_{n=2}^{\infty} n(n-1) \frac{\langle n \rangle^n e^{-\langle n \rangle}}{n!} \qquad \text{A.8}$$

and the $n(n-1)$ cancels with part of the $n!$ to give

$$\langle n^2 \rangle = \langle n \rangle + \langle n \rangle^2 \sum_{n=2}^{\infty} \frac{\langle n \rangle^{n-2} e^{-\langle n \rangle}}{(n-2)!}, \qquad \text{A.9}$$

where $\langle n \rangle^2$ has been pulled out of the summation. By making the change of variables $m = n - 2$, Equation A.9 becomes

$$\begin{aligned}\langle n^2\rangle &= \langle n\rangle + \langle n\rangle^2 \sum_{m=0}^{\infty} \frac{\langle n\rangle^m e^{-\langle n\rangle}}{(m)!} \\ &= \langle n\rangle + \langle n\rangle^2 \sum_{m=0}^{\infty} P_T(m) \\ &= \langle n\rangle + \langle n\rangle^2\end{aligned} \qquad \text{A.10}$$

Substituting this into Equation A.3,

$$\begin{aligned}\sigma^2 &= \langle n^2\rangle - \langle n\rangle^2 \\ &= \langle n^2\rangle + \langle n\rangle - \langle n^2\rangle. \\ &= \langle n\rangle\end{aligned} \qquad \text{A.11}$$

Therefore the variance of a Poisson process is equal to the mean.[1]

Equation A.11 gives the variance in terms of the number of photons detected, but the SNR is in terms of mean square current. Equation A.11 can be used to arrive at the current variance to be used in the SNR equation. The mean squared shot noise current from the detector is defined as the variance of the current [3]

$$\langle i_q^{\,2}\rangle = \sigma_{curr}^{\,2} = \langle (i - \langle i\rangle)^2\rangle \qquad \text{A.12}$$

where i is the current in any time interval, given by the number of photons in the time interval multiplied by the charge on an electron, e, and divided by the time,

$$i = \frac{ne}{T}. \qquad \text{A.13}$$

In Equation A.12, $\langle i\rangle$ is the average current flow per time interval for a large sampling,

$$\langle i \rangle = \frac{\langle n \rangle e}{T}. \qquad \text{A.14}$$

Using Equations A.11, A.12, A.13 and A.14, the mean square shot noise current is

$$\overline{i_q^2} = \frac{e}{T}\langle i \rangle. \qquad \text{A.15}$$

Since the sample time is equal to one over twice the effective bandwidth,[1,3]

$$T = \frac{1}{2B_e}, \qquad \text{A.16}$$

the mean square shot noise current becomes

$$\overline{i_q^2} = 2eB_e\bar{i}. \qquad \text{A.17}$$

This analysis has shown the mean square shot noise is proportional to the number of photons incident on the detector. This result agrees with the physical observation that the shot noise from a detector increases as the amount of incident light is increased.

BIBLIOGRAPHY

[1] G. Keiser, Optical Fiber Communications, McGraw-Hill, 1991.

[2] C. G. Bachman, Laser Radar Systems and Techniques, Artech House, Inc., 1979.

[3] K. D. Moller, Optics, University Science Books, 1988.

[4] R. L. Schwiesow and R. F. Calfee, "Atmospheric Refractive Effects on Coherent Lidar Performance at 10.6 μm", Applied Optics, Vol. 18, No. 23, December 1979, pp 3991.

[5] V. E. Derr and C. G. Little, "A Comparison of Remote Sensing of the Clear Atmosphere by Optical, Radio and Acoustic Radar Techniques", Applied Optics, Vol. 9, No. 9, September 1970, pp 1976.

[6] T. R. Lawrence, R. M. Huffaker, F. F. Hall, Jr., and P. A. Mandics, "Considerations of a Satellite-Borne Global Wind Sensing Coherent Lidar", OSA Annual Meeting, November 1978.

[7] R. L. Schwiesow, R. E. Cupp, M. J. Post and R. F. Calfee, "Coherent Differential Doppler Measurements of Transverse Velocity at a Remote Point", Applied Optics, Vol. 16, No. 5, May 1977, pp 1145.

[8] M. J. Post, "Effects of the Earth's Atmosphere on a Spaceborne IR Doppler Wind-Sensing System", Applied Optics, Vol. 18, No. 15, August 1979, pp 2645.

[9] M. P. McCormick, "Lidar in Space", OSA Optical Remote Sensing of the Atmosphere Conference, February 1990, 1990 Technical Digest Series Volume 4, pp 67.

[10] F. F. Hall, Jr., "Remote Sensing of Airborne Hydrocarbons and Toxic Pollutants - Present Status and Future Projections", OSA Optical Remote Sensing of the Atmosphere Conference, February 1990, 1990 Technical Digest Series Volume 4, pp 320.

[11] T. Flom, "Spaceborne Laser Radar", Applied Optics, Vol. 11, No. 2, February 1979, pp 291.

BIBLIOGRAPHY
-Continued-

[12] P. Hermet, "Design of a Rangefinder for Military Purposes", Applied Optics, Vol. 11, No. 2, February 1972, pp 273.

[13] C. R. Cooke, "Automatic Laser Tracking and Ranging System", Applied Optics, Vol. 11, No. 2, February 1972, pp 277.

[14] M. Elbaum and Paul Diament, "Estimation of Image Centroid, Size and Orientation with Laser Radar", Applied Optics, Vol. 16, No. 9, September 1977, pp 2433.

[15] S. W. Henderson, C. P. Hale, P. J. M. Suni, and J. R. Magee, "Solid-State Coherent Laser Radar Technology at 2 μm: Current Status and Future Prospects", OSA Coherent Laser Radar Technology and Applications Conference, July 1991, 1991 Technical Digest Series Vol. 12.

[16] P. F. Moulton, J. Harrison, J. H. Flint, and D. M. Rines, "Solid State Lasers for Coherent Laser Radar", OSA Coherent Laser Radar Technology and Applications Conference, July 1991, 1991 Technical Digest Series Vol. 12.

[17] B. T. McGuckin and R. T. Menzies, "Efficient High Peak Power Output from Tunable Diode-pumped Q-switched 2μm Tm,Ho:YLF laser", OSA Coherent Laser Radar Technology and Applications Conference, July 1991, 1991 Technical Digest Series Vol. 12.

[18] L. N. Durvasula, "1 and 2 Micron Laser Radar Transmitter Development," OSA Coherent Laser Radar Technology and Applications Conference, July 1991, Technical Digest Series, Vol. 12.

[19] R. Barbini, "Italian CO_2 Lidar Work and Laser Development," OSA Coherent Laser Radar Technology and Applications Conference, July 1991, Technical Digest Series, Vol. 12.

[20] S. F. Carter, D. Szebesta, S. T. Davey, R. Wyatt, M. C. Brierley and P. W. France, "Amplification at 1.3 μm in a Pr^{3+}-doped single-mode fluorozirconate fiber", *Electronic Letters*, vol. 27, 1991, pp 628-629.

[21] R. Olshansky, "Noise Figure for Erbium Doped Optical Fibre Amplifiers," Electronics Letters, Vol. 24, 1988, pp1363-1365.

[22] P. W. France, *Optical Fibre Lasers & Amplifiers*, Blackie and Son Ltd., Glasgow and London, 1991.

BIBLIOGRAPHY
-Continued-

[23] E. Snitzer, "Rare Earth Doped Fiber Lasers," *Optical Fiber Communications '92 Conference Tutorial Sessions*, Tutorial FE, pp 418-484, February 4-7, 1992.

[24] R. E. Miers, "Fiber Laser Preamplifier for Laser Radar Detectors," *1991 USAF-RDL Summer Faculty Research Program Reports*, Volume 5.B, Wright Laboratory Report 26, Wright Patterson Air Force Base, Ohio, July 1991.

[25] A. V. Jelalian, *Laser Radar Systems*, Artech House, p. 32 Table 1.1, Boston, 1992

[26] G. E. Keiser, *Optical Fiber Communications, Second Edition*, McGraw-Hill, Inc., p 244, New York, 1991.

[27] See, for example, E. L. Dereniak and D. G. Crowe, *Optical Radiation Detectors*, John Wiley & Sons, New York, 1984

[28] See, for example, R. W. Boyd, *Radiometry and the Detection of Optical Radiation*, John Wiley & Sons, New York, 1983

[29] W. L. Wolfe and G. J. Zissis, *The Infrared Handbook*, table 21-3, Infrared Information and Analysis Center at Environmental Research Institute of Michigan, compiled for the Office of Naval Research, Department of the Navy, revised 1985.

[30] R. H. Kingston, *Detection of Optical and Infrared Radiation*, chapt. 8, Springer-Verlag, New York, 1978.

[31] N. A. Olsson, "Lightwave Systems with Optical Amplifiers," *Journal of Lightwave Technology*, Vol. 7, No. 7, 1071-1082, July1989.

[32] M. S. Salisbury, P. F. McManamon, and B. D. Duncan, "Signal to Noise Ratio Improvement of a One Micron Ladar System Incorporating an Optical Fiber Preamplifier," *Optical Engineering*, Vol. 32, No. 11, November 1993

VITA

July 21, 1968	Born - Macomb, Illinois
1987	Physics Division Lab Assistant, North Central College, Naperville, Illinois
1988	Co-op Student Employee, Argonne National Laboratory, Argonne Tandem Linear Accelerator System, ATLAS Operations Group
1990	B.A., North Central College, Naperville, Illinois
1990	Research Assistant, University of Dayton at Wright Patterson AFB, Dayton, Ohio
1992	Junior Electro-Optic Engineer, Technology/Scientific Services, Inc. at Wright Patterson AFB, Dayton, Ohio
1993	M.S., University of Dayton, Dayton, Ohio

PUBLICATIONS

Optical Fiber Preamplifiers for Ladar Detection and Associated SNR Improvement Measurements, (To be submitted December 93 Optical Engineering).

Signal to Noise Ratio Improvement of a One Micron Ladar System Incorporating an Optical Fiber Preamplifier, Optical Engineering, November 1993, Authored.

Signal to Noise Ratio Improvement in Lidar Systems Incorporating Neodymium Doped Optical Fiber Preamplifiers, Proceedings of the National Aerospace Electronics Conference (NAECON), Dayton, Ohio, May 1992, Authored and Presented.

-continued-

Coherent 1.06 Micron Laser Radar for Fiber Preamplifier Research, The International Society for Optical Engineering - LASERS '92, Los Angeles, California, February 1992, Co-authored.

Coherent 1.06 Micron System for Liquid Crystal Beam Steerer Evaluation, IRIS Specialty Group on Active Systems, Silver Spring, Maryland, October 1991 Co-authored.

Neodymium Doped Fiber Amplifier in Lidar Detection, Optical Society of America - OPTCON '91, San Jose California, November 1991, Presented.